A sensitivity theory for the equilibrium boundary layer over land

Timothy W. Cronin[1]

Received 11 April 2013; revised 24 July 2013; accepted 16 September 2013; published 4 November 2013.

[1] Due to the intrinsic complexities associated with modeling land-atmosphere interactions, global models typically use elaborate land surface and boundary layer physics parameterizations. Unfortunately, it is difficult to use elaborate models, by themselves, to develop a deeper understanding of how land surface parameters affect the coupled land-atmosphere system. At the same time, it is also increasingly important to gain a deeper understanding of the role of changes in land cover, land use, and ecosystem function as forcings and feedbacks in past and future climate change. To improve the foundation of our understanding, we outline a framework for boundary layer climate sensitivity based on surface energy balance; just as global climate sensitivity is based on top-of-atmosphere energy balance. We develop an analytic theory for the boundary layer climate sensitivity of an idealized model of a diurnally averaged well-mixed boundary layer over land. This analytic sensitivity theory identifies changes in the properties of the land surface—including moisture availability, albedo, and aerodynamic roughness—as forcings, and identifies strong negative feedbacks associated with the surface fluxes of latent and sensible heat. We show that our theory can explain nearly all of the sensitivity of the Betts (2000) full system of equations. Favorable comparison of the theory and the simulation results from a two-column radiative convective model suggests that the theory may be broadly useful for unifying our understanding of how changes in land use or ecosystem function may affect climate change.

Citation: Cronin, T. W. (2013), A sensitivity theory for the equilibrium boundary layer over land, *J. Adv. Model. Earth Syst.*, *5*, 764–784, doi:10.1002/jame.20048.

1. Introduction

[2] Global-mean surface air temperature is controlled primarily by planetary energy balance, in which greenhouse gas concentrations and the planetary albedo play a dominant role. Simple models of the sensitivity of planetary energy balance to greenhouse gas concentrations form the foundation of our understanding of how well-mixed greenhouse gases, such as anthropogenic CO_2, affect global climate. Land surface properties, such as moisture availability and roughness, play less of a role in determining the global-mean surface temperature, but they can strongly affect local surface temperatures, with disproportionately large impacts on society. The potential importance of climate change forced by land surface changes ought to be a concern in any comprehensive study of climate change, because the human footprint on the land surface is large, and rapidly changing.

[3] In order to both simulate and understand important problems related to the climate system, *Held* [2005] argues for the importance of model hierarchies, with models that span a range of complexity levels. Since the early and influential studies of *Charney* [1975] and *Shukla and Mintz* [1982], much valuable work has been done to simulate the impacts of the land surface on the climate (and vice versa) with highly complex general circulation models (GCMs). Toward the simpler end of the complexity spectrum, idealized models of the coupled surface-boundary layer system have done a great deal to advance our understanding of land-atmosphere interactions [e.g., *McNaughton and Spriggs*, 1986; *Jacobs and De Bruin*, 1992; *Brubaker and Entekhabi*, 1995; *Kim and Entekhabi*, 1998]. One of the central motivations of this work is our belief that the existing model hierarchies in the field of land-atmosphere interactions do not extend down to models that are sufficiently simple so as to be analytically tractable, and that the lack of analytic models and frameworks impedes the understanding and synthesis of results from more complex models. Despite the large body of work with both simple and complex models, there remains no widely accepted corollary to climate

[1]Program in Atmospheres, Oceans, and Climate, Massachusetts Institute of Technology, Cambridge, MA, 02139, USA.

Corresponding author: T. W. Cronin, Program in Atmospheres, Oceans, and Climate, Massachusetts Institute of Technology, 77 Massachusetts Ave., Cambridge, MA 02139, USA. (twcronin@mit.edu)

1942-2466/13/10.1002/jame.20048

sensitivity when it comes to understanding the impact of land surface properties on changes in near-surface temperatures.

[4] In this study, we attempt to define such a corollary to climate sensitivity, by introducing the framework of boundary layer climate sensitivity. We suggest that daily-average regional temperature response due to changes in surface moisture availability, albedo, and roughness can be understood within a context of forcings and feedbacks, similar to the case of global climate response to a radiative perturbation, but based on surface energy balance, rather than top-of-atmosphere energy balance. Many of the aspects of our work are not new; numerous other studies have used the language of sensitivity theory to describe feedbacks (and occasionally forcings) in the coupled land-atmosphere system. Because of the importance of the diurnal cycle for land-atmosphere exchanges of water, energy, and momentum, such studies have often focused on the role of feedbacks in the evolution of temperature and evaporation over only a single day [*Jacobs and De Bruin*, 1992; *van Heerwaarden et al.*, 2009, 2010]. In such work, initial conditions are often of major importance, and model results are compared to observations of weather, rather than climate.

[5] Our work focuses on longer time scales, emphasizing the importance of land surface properties in determining daily-average surface and boundary layer temperatures. Because of the relative unimportance of the diurnal cycle for ocean-atmosphere coupling, the equilibrium climate of the surface-boundary layer system over the ocean is more easily defined, observed, and modeled [*Betts and Ridgway*, 1988, 1989]. The problem of the daily-average state of the coupled surface-boundary layer system over land was tackled later, first by models with fixed boundary layer depth [*Brubaker and Entekhabi*, 1995; *Entekhabi and Brubaker*, 1995; *Brubaker and Entekhabi*, 1996], then by models with variable boundary layer depth [*Kim and Entekhabi*, 1998; *Betts*, 2000]. The elegant studies of *Entekhabi and Brubaker* [1995] and *Brubaker and Entekhabi* [1996] used an idealized model to explore the feedbacks that serve to amplify or dampen forced soil moisture and temperature variability over time scales of days to months. However, the temperature variability in their work was forced by wind speed, rather than any changes in land surface properties, and their assumption of constant boundary layer height cuts the important connection between warming and boundary layer deepening, as well as any control on boundary layer temperatures exerted by the free troposphere. Our work will build off the diurnally averaged mixed layer-surface model of *Betts* [2000], which has a very simple treatment of radiation and surface turbulent exchange, but relaxes the constant-height assumption of *Brubaker and Entekhabi* [1995] and the constant specific humidity assumption of *Kim and Entekhabi* [1998].

[6] Based on the model of *Betts* [2000], we derive analytic expressions for the response of surface temperature and boundary layer potential temperature to forcing by perturbations in surface moisture availability, albedo, and roughness. As in the studies of *Brubaker and Entekhabi* [1996] and *Kim and Entekhabi* [1998], our theory associates the strongest negative feedback with the dependence of the surface latent heat flux on saturation vapor pressure. We compare the results from our analytic theory to the full model of *Betts* [2000] and show that our theory can explain nearly all of the sensitivity of the *Betts* [2000] full system of equations. As in the case of the nonlinear (approximately logarithmic) radiative forcing by CO_2, we find that allowance for nonlinear forcing functions is important, especially for large changes in surface moisture availability and roughness. We find that the theory agrees well with simulation results from a more complex two-column radiative-convective model, and we discuss limitations of the theory. We conclude by discussing how our theory may allow for a more unified understanding of the boundary layer climate response to disparate problems such as urbanization, deforestation, drought, and CO_2-induced stomatal closure.

2. Theory

2.1. Framework for Boundary Layer Sensitivity

[7] Top-of-atmosphere radiative energy balance serves as the guiding principle in the theory of global climate sensitivity:

$$R_S - R_L = 0, \tag{1}$$

where R_S is the top-of atmosphere net downward shortwave radiation absorbed by the Earth, and R_L is the top-of-atmosphere net longwave radiation emitted by the Earth. To understand how an arbitrary forcing parameter, A (e.g., CO_2), affects the climate near a known reference state, we take the total derivative of top-of-atmosphere energy balance with respect to A:

$$\frac{\mathrm{d}R_S}{\mathrm{d}A} - \frac{\mathrm{d}R_L}{\mathrm{d}A} = 0. \tag{2}$$

[8] We expand the total derivatives into forcings (e.g., $\partial R_L/\partial A$), plus products of feedbacks and responses (e.g., $(\partial R_L/\partial T)(dT/dA)$, where T represents global temperature), and then solve for the response as the sum of forcings divided by the sum of feedbacks. Such a decomposition of the climate response to increasing concentrations of well-mixed greenhouse gases has helped us to standardize model simulations, focus study on key mechanisms that mediate the strength of the climate response, and identify ways in which models resemble or differ from one another.

[9] We propose a similar framework for boundary-layer climate sensitivity, with a guiding principle of surface energy balance. Assuming a long-term equilibrium with no subsurface heat flux, surface energy balance is given by

$$Q_S - Q_L - H - E = 0, \tag{3}$$

where Q_S is the net shortwave radiation at the surface (positive downward), Q_L is the net longwave radiation

at the surface (positive upward), E is the latent heat flux, and H is the sensible heat flux (both defined to be positive upward). To apply a sensitivity framework to the problem, we begin by taking the total derivative of (3) with respect to the arbitrary variable A, near a well-defined reference state of the surface-boundary layer system, where surface energy balance holds:

$$\frac{\mathrm{d}Q_S}{\mathrm{d}A} - \frac{\mathrm{d}Q_L}{\mathrm{d}A} - \frac{\mathrm{d}H}{\mathrm{d}A} - \frac{\mathrm{d}E}{\mathrm{d}A} = 0. \tag{4}$$

[10] Expansion of each of these total derivatives by the chain rule is algebraically complicated and requires us to define which controlling variables to include in our expansion of (4). We suggest that the set of controlling variables should include at least the ground temperature, T_S, the near-surface potential temperature of the boundary layer, θ_M, and the near-surface specific humidity of the boundary layer, q_M (these are also three of the prognostic variables in the idealized model of *Brubaker and Entekhabi* [1995]). Variables related to cloudiness, especially low-level cloud fraction and water path, may also be quite important, but we will not consider them explicitly in our example case below.

[11] Once such a set of controlling variables is defined, we can define a boundary layer climate sensitivity by:

[12] 1. Eliminating all but one controlling variable by identifying relationships among them (e.g., by linearly relating changes in T_S and q_M to changes in θ_M)

[13] 2. Evaluating, theoretically or empirically, the partial derivatives of the surface fluxes with respect to the controlling variables (terms such as $\partial E/\partial T_S$)

[14] 3. Algebraically rearranging to solve for how changes in a controlling variable are affected by changes in a forcing variable, δA

[15] The framework proposed here may seem abstract and somewhat open ended, but this is intended for generality. In order to apply this framework to a GCM, one would likely have to conduct a suite of perturbation experiments. The relationships among controlling variables, as well as the partial derivatives of surface fluxes with respect to controlling variables, could be evaluated by multiple linear regression.

[16] In order to provide a more concrete example of the proposed framework, the remainder of the theory section will be devoted to deriving the boundary layer sensitivity of a highly idealized model of the equilibrium boundary layer, as presented by *Betts* [2000]. With appropriate simplifications and assumptions, it will turn out that we can actually arrive at an analytic expression for the sensitivity of the equilibrium boundary layer to forcing by changes in various surface parameters. For the convenience of a reader who is interested in our ideas but not our detailed derivation, we include the key equations from the analytic sensitivity theory (sections 2.2–2.7) in Tables 1 and 2.

2.2. Equilibrium Boundary Layer Model of Betts [2000]

[17] Following the work by *Betts* [2000] (hereafter B00), we seek to understand the problem of the surface-atmosphere interaction by considering equations for the time-mean surface temperature T_S, and the time-mean boundary layer potential temperature and specific humidity, θ_M and q_M, in a well-mixed boundary layer (ML) (see Figure 1 for a schematic of the thermal structure). Here, we review some of the key model assumptions from B00.

[18] Following commonly used conventions [e.g., *Allen et al.*, 1998; *Jones*, 1992], B00 defines bulk formulae for the latent and sensible heat fluxes E and H as follows:

$$E = \rho L_v \frac{g_a g_v}{g_a + g_v} (q^*(T_S) - q_M), \tag{5}$$

$$H = \rho c_p g_a (T_S - \theta_M), \tag{6}$$

where ρ is the density of air, L_v is the latent heat of vaporization of water, c_p is the specific heat capacity of air, $q^*(T_S)$ is the saturation mixing ratio of water vapor at surface temperature (for simplicity, we assume that the surface pressure equals the reference pressure in the definition of θ). The surface conductance to sensible heat flux, g_a (units: m/s), can be written as the product of a nondimensional enthalpy flux coefficient, c_k, and a surface wind speed, $|\mathbf{v_s}|$:

Table 1. Key Equations From the Analytic Sensitivity Theory of Sections 2.2–2.7

Description	Expression	Equation Number
General sensitivity equation	$\delta\theta_M = -\frac{F^A_{Q_L} + F^A_E - F^A_{Q_S}}{\lambda_H + \lambda_E + \lambda_{Q_L} - \lambda_{Q_S}}$	(22)
Sensible heat flux feedback	$\lambda_H = \rho c_p g_a \gamma$	(25)
Evaporative feedback	$\lambda_E = \rho L_v \frac{g_a g_v}{g_a + g_v} \frac{\partial q^*}{\partial T}\Big\|_{T_{S0}} \left[1 + \gamma - \xi \left(\frac{\partial q^*}{\partial T}\right)^{-1}\right]$	(26)
Longwave feedback	$\lambda_{Q_L} = 4\sigma_B T^3_{S0} \gamma$	(27)
Relationship between δT_S and $\delta\theta_M$	$\delta T_S = -\frac{1}{\rho c_p g_a} \frac{\partial H}{\partial A} \delta A + (1+\gamma)\delta\theta_M$	(16)
Relationship between δq_M and $\delta\theta_M$	$\delta q_M = \xi \delta\theta_M$	(20)
Parameter relating δT_S to $\delta\theta_M$	$\gamma = \frac{\overline{Qz}}{\rho g_a g \Gamma (1+k)}$	(17)
Parameter relating δq_M to $\delta\theta_M$	$\xi = \left[\frac{\partial q^*}{\partial T}\Big\|_{T_b} \left(\frac{p_s}{p_b}\right)^{\frac{R}{c_p}} \left(1 - \frac{R\theta_M}{c_p p_b \Gamma}\right) + \frac{q_M}{p_b \Gamma}\right]$	(21)

Table 2. Nonlinear Forcings From Sections 2.5–2.7

Forcing Term	$A \to g_v$	$A \to \alpha$	$A \to g_a$
Longwave forcing $\left(F^A_{Q_L}\right)$	0	0	$\frac{4\sigma_B T^3_{S0} H_0}{\rho c_p}\left(\frac{1}{g_a}-\frac{1}{g_{a0}}\right)$ (36)
Shortwave forcing $\left(F^A_{Q_S}\right)$	0	$-\frac{Q_{S0}}{1-\alpha_0}(\alpha-\alpha_0)$ (32)	0
Evaporative forcing $\left(F^A_E\right)$	$E_0 \ln\left(\frac{g_v}{g_{v0}}\frac{g_{a0}+g_{v0}}{g_a+g_v}\right)$ (29)	0	$\left(E_0-\frac{H_0}{B_e}\right)\ln\left(\frac{g_a}{g_{a0}}\frac{g_{a0}+g_{v0}}{g_a+g_v}\right)$ (37)

$$g_a = c_k |\mathbf{v_s}|. \tag{7}$$

[19] The surface conductance to water vapor, g_v (units: m/s), represents the limited availability of water for evaporation over land; viewed as a resistance, g_v^{-1} describes the additional path though which water within a leaf (or under the soil) must diffuse in order to arrive at the outermost layer of the leaf (or soil surface) and enter the atmosphere. The total conductance to latent heat flux, $g_a g_v/(g_a+g_v)$, is equivalent to the total conductance of two conductors in series, and can alternatively be viewed as a product of the conductance to sensible heat flux, g_a, and a dimensionless evaporative efficiency:

$$\beta \equiv g_v/(g_a+g_v). \tag{8}$$

[20] The evaporative efficiency β can vary between limits of 0 ($g_v=0$, completely dry surface, no latent heat flux) and 1 ($g_v \to \infty$, completely wet surface, identical exchange coefficients for sensible and latent heat fluxes). Over a vegetated surface, g_v is primarily determined by the number, size, and openness of the numerous leaf pores, or stomata, of the canopy. If the atmospheric inputs, including the surface radiative fluxes, are considered as given, the three equations (3), (5), and (6) can be solved simultaneously for the three unknowns: the two components of the surface enthalpy flux and the surface temperature. By assuming the surface-air temperature difference is small, the latent heat flux equation can be linearized, and the system can be solved analytically; this gives the well-known Penman-Monteith equation [*Monteith*, 1965].

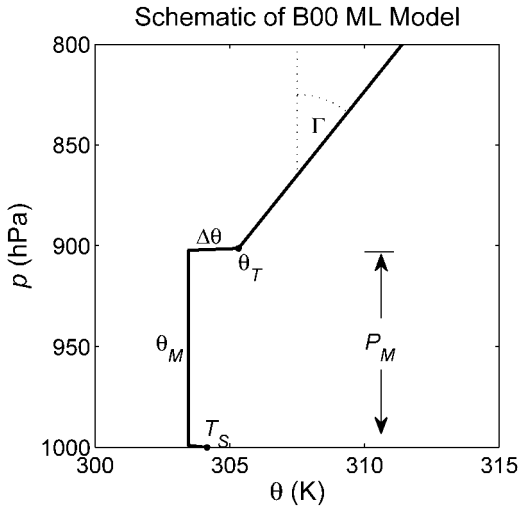

Figure 1. Schematic of thermal structure in *Betts* [2000] equilibrium boundary layer model.

[21] In addition to equations for bulk fluxes and surface energy balance, B00 uses equations for ML moisture and energy balance, and two equations for the jumps $\Delta\theta$ and Δq just above the top of the ML. A key difference between the model of B00 and that of *Brubaker and Entekhabi* [1995] is that B00 prescribes boundary conditions just above the top of the ML for θ and q, which depend on the pressure thickness of the ML (ML height in *Brubaker and Entekhabi* [1995] is fixed). The upper boundary condition on θ is important to our theory and discussed below in more detail. The upper boundary condition on q is relatively unimportant to our theory, and we only mention it here briefly: air just above the top of the ML, with potential temperature and specific humidity (θ_T, q_T), is assumed to have a prescribed saturation point deficit $\mathcal{P}_T$, or pressure distance that must be lifted to reach its LCL. B00 also uses two closures that are important for our theory; one relates the ML-top downward buoyancy flux to the surface buoyancy flux, and the other states that the ML extends upward to the lifted condensation level (LCL) of air in the ML (both are discussed below in more detail). Our derivation in section 2.3 requires the energy balance equation, upper boundary condition on θ, and the LCL closure; we also use the buoyancy flux closure, but apply it without the virtual temperature correction for simplicity, as in *Tennekes* [1973].

[22] In the absence of advective tendencies, the leading-order energetic balance in the ML is between sensible heat flux convergence and net radiative cooling (B00, *Takahashi* [2009]). However, since we want to allow for deep precipitating convection over land in our simulations, we follow B00 and also include a term for convective cooling of our reference state ML, which consists of the combination of latent cooling by evaporating rainfall and sensible cooling by penetrative downdrafts. Defining $\overline{Q_C}$ as the ML average convective cooling rate, and $\overline{Q_R}$ as the ML average radiative cooling rate, we introduce a total convective plus radiative average cooling rate (units: K/s) for the boundary layer:

$$\overline{Q_\Sigma} = \overline{Q_R} + \overline{Q_C}. \tag{9}$$

[23] Then, using the *Tennekes* [1973] closure of linking ML-top sensible heat flux to surface sensible heat flux, we can write the ML thermal balance as

$$(1+k)H = \frac{c_p \overline{Q_\Sigma} P_M}{g}, \tag{10}$$

where k is a coefficient relating the downward sensible heat flux at the top of the ML to the surface sensible heat flux (typically $\sim$0.2; *Tennekes* [1973]), and P_M is the pressure thickness of the ML. As in B00, P_M is assumed to be given by the difference between the surface pressure (p_s) and the pressure at the lifted condensation level of air in the boundary layer:

$$P_M = p_s - p_{LCL}(\theta_M, q_M). \tag{11}$$

[24] The closure that the top of the ML lies at the LCL is consistent with a shallow cumulus mass flux (out of the ML) that is nearly zero if the top of the ML is subsaturated, but increases very strongly as the top of the ML reaches supersaturation. This closure also assumes that a nonzero shallow cumulus mass flux out of the ML is required to balance the ML water budget; this assumption may break down if the ML is very deep and dry, or if subsidence very strong, or if the air above the top of the ML is extremely dry. We also assume that the potential temperature just above the top of the ML, θ_T, has a known profile:

$$\theta_T = \theta_{00} + \Gamma(P_M - P_{00}), \tag{12}$$

where θ_{00} is the potential temperature of the free troposphere just above a ML with reference thickness P_{00}, and Γ is the absolute value of the lapse rate of potential temperature in pressure coordinates (K/Pa). The boundary layer potential temperature is related to θ_T by

$$\theta_M = \theta_T - \Delta\theta. \tag{13}$$

[25] Equations (10), (11), (12), and (13) correspond to B00 equations (16), (21), (12), and (10), respectively.

[26] To solve for the ML thermal structure and fluxes, B00 further requires a moisture budget equation, as well as equations for ML-top jumps and fluxes that result in a balance between mass addition to the ML by entrainment, and mass removal from the ML by the combination of subsidence and a shallow convective mass flux. The mass balance requirement warms and dries the ML by replacing ML air (θ_M, q_M) with free-tropospheric air (θ_T, q_T). We will proceed without these additional expressions in our sensitivity theory, due to the observation that in the results of B00, changes in $\Delta\theta$ are much smaller than changes in θ_M, typically by roughly a factor of 10 (see B00 Figure 4a as compared to 3a). This observation can be used to outline the route to the analytic sensitivity theory that we will take. Informally, based on (13), the smallness of changes in the jump $\Delta\theta$ implies that $\delta\theta_M \approx \delta\theta_T$, and together with (12), we have $\delta\theta_M \approx \Gamma\delta P_M$. Along with (10) and (11), this allows us to link changes in θ_M to changes in T_S and q_M. With the enthalpy flux definitions and surface energy balance, we can then determine the sensitivity of θ_M to changes in an arbitrary variable A that affects the surface energy budget. Before assuming anything specific about the forcing agent A, we will first proceed through most of this derivation (section 2.3), and also discuss the key feedbacks in the system (section 2.4). We will then discuss the specific cases of forcing by changes in surface conductance to water vapor, surface albedo, and surface aerodynamic conductance (sections 2.5, 2.6, and 2.7, respectively). Our specific choice of three land surface parameters stems in part from past studies; *McNaughton and Spriggs* [1986] and *Jacobs and De Bruin* [1992] both explored the sensitivity of boundary layer growth and evaporation over a single day to the surface resistance (r_s), net radiation ($Q^* = Q_S - Q_L$), and aerodynamic resistance (r_a). Each of these parameters maps cleanly to one of our land surface parameters; surface resistance is the reciprocal of vegetation conductance ($r_s = 1/g_v$), surface net radiation is directly affected by albedo ($Q^* = (1-\alpha)Q_S^{\downarrow} - Q_L$), and surface aerodynamic resistance is the reciprocal of aerodynamic conductance ($r_a = 1/g_a$).

2.3. Analytic Sensitivity Theory for B00 Model

[27] We expand the total derivative of surface energy balance with respect to A (4) using the chain rule (see Appendix A2; (A4)–(A7)). This expansion yields terms containing factors of $\mathrm{d}T_S/\mathrm{d}A$ and $\mathrm{d}q_M/\mathrm{d}A$; we seek to eliminate both of these in favor of $\mathrm{d}\theta_M/\mathrm{d}A$, thus allowing us to solve for $\mathrm{d}\theta_M/\mathrm{d}A$.

[28] To obtain the relationship between $\mathrm{d}T_S/\mathrm{d}A$ and $\mathrm{d}\theta_M/\mathrm{d}A$, we differentiate (10) with respect to A (also using the chain rule expansion of $\mathrm{d}H/\mathrm{d}A$):

$$\frac{\partial H}{\partial A} + \rho c_p g_a \left(\frac{\mathrm{d}T_S}{\mathrm{d}A} - \frac{\mathrm{d}\theta_M}{\mathrm{d}A} \right) = \frac{c_p \overline{Q_\Sigma}}{g(1+k)} \frac{\mathrm{d}P_M}{\mathrm{d}A}. \tag{14}$$

[29] Here, we have assumed that k does not depend on A, and (as in B00) that the changes in integrated cooling of the boundary layer are dominated by changes in the pressure depth of the boundary layer, P_M, rather than by changes in the average ML cooling rate, $\overline{Q_\Sigma}$. This is a somewhat inaccurate assumption in a model with full radiative transfer and convection parameterizations, as the ML depth typically affects its cooling rate by both radiation and convection; this limitation will be discussed later. As discussed above, we next assume that changes in the jump $\Delta\theta_M$ are small, so that

$$\frac{\mathrm{d}\theta_M}{\mathrm{d}A} = \frac{\mathrm{d}\theta_T}{\mathrm{d}A} - \frac{\mathrm{d}\Delta\theta}{\mathrm{d}A} \approx \frac{\mathrm{d}\theta_T}{\mathrm{d}A} = \Gamma \frac{\mathrm{d}P_M}{\mathrm{d}A}, \tag{15}$$

[30] Applying (15) to (14) to eliminate $\mathrm{d}P_M/\mathrm{d}A$, and rearranging to isolate $\mathrm{d}T_S/\mathrm{d}A$, gives the relationship we sought between $\mathrm{d}T_S/\mathrm{d}A$ and $\mathrm{d}\theta_M/\mathrm{d}A$:

$$\frac{\mathrm{d}T_S}{\mathrm{d}A} = -\frac{1}{\rho c_p g_a} \frac{\partial H}{\partial A} + (1+\gamma) \frac{\mathrm{d}\theta_M}{\mathrm{d}A}, \tag{16}$$

where we have defined γ as follows for notational convenience:

$$\gamma \equiv \frac{\overline{Q_\Sigma}}{\rho g_a g \Gamma (1+k)}. \tag{17}$$

[31] This nondimensional parameter, γ, relates changes in T_S and θ_M (typically $\gamma \sim 0.2$). If A does not

directly affect H, then changes in T_S are just linearly related to changes in θ_M, with the proportionality constant $(1+\gamma)$.

[32] Obtaining the relationship between $\mathrm{d}q_M/\mathrm{d}A$ and $\mathrm{d}\theta_M/\mathrm{d}A$ simply involves careful application of the closure (11) from B00, which assumes the top of the ML coincides with the LCL. First, we note that q_M is equal to $q^*(T_b, p_b)$, where T_b is the temperature at the top of the ML, and p_b is the pressure at the top of the ML ($p_b = p_s - P_M$):

$$T_b = \theta_M (p_b/p_s)^{(R/c_p)}. \tag{18}$$

[33] This means that

$$\frac{\mathrm{d}q_M}{\mathrm{d}A} = \frac{\mathrm{d}}{\mathrm{d}A}\left(\frac{\epsilon e^*(T_b)}{p_b}\right), \tag{19}$$

where e^* is the saturation vapor pressure at T_b. Using (15), we can eliminate $\mathrm{d}p_b/\mathrm{d}A = -\mathrm{d}P_M/\mathrm{d}A$ from the expansion of (19) (see Appendix A1 for details):

$$\frac{\mathrm{d}q_M}{\mathrm{d}A} = \xi \frac{\mathrm{d}\theta_M}{\mathrm{d}A}, \tag{20}$$

where for notational purposes, we have defined ξ as follows:

$$\xi \equiv \left[\frac{\partial q^*}{\partial T}\Big|_{T_b}\left(\frac{p_s}{p_b}\right)^{\frac{R}{c_p}}\left(1 - \frac{R\theta_M}{c_p p_b \Gamma}\right) + \frac{q_M}{p_b \Gamma}\right]. \tag{21}$$

[34] Our definition of ξ includes the reminder that the partial derivative of q^* with respect to T is evaluated at (T_b, p_b), because other instances of $\partial q^*/\partial T$ that will later appear are evaluated at surface temperature and pressure. While the expression for ξ is cumbersome, all of the terms in it should be known straightforwardly from the reference state. Unless the atmosphere is extremely stable (i.e., Γ is very large), ξ is negative; as long as free-tropospheric temperatures decrease with height, a deeper, warmer ML still has colder ML-top temperature. Since ML-top temperature is the primary control on saturation mixing ratio, this implies q_M must decrease as θ_M increases. If the lapse rate above the ML is approximately moist adiabatic, then saturation static energy $\left(L_v q^* + c_p T + gz\right)$ is nearly constant with height, and it follows that $\xi \approx -c_p/L_v$.

[35] We can now return to (4), applying (16) and (20) to solve for $\mathrm{d}\theta_M/\mathrm{d}A$; as the algebra is somewhat cumbersome, details of the derivation are given in Appendix A2. We can then cast the expression into finite-difference form to get $\delta\theta_M \equiv \theta_M - \theta_{M0}$ in terms of $\delta A \equiv A - A_0$, giving forcings that are linear in the perturbation δA (zeros represent reference-state values; linear forcings are defined by (A15)). Alternatively, we can integrate to obtain forcings that are nonlinear functions of A and A_0 (nonlinear forcings are defined by (23)). Either way, we can rearrange our solution for $\mathrm{d}\theta_M/\mathrm{d}A$ to obtain a response-forcing-feedback expression:

$$\delta\theta_M = \frac{F^A_{Q_S} - F^A_{Q_L} - F^A_E}{\lambda_H + \lambda_E + \lambda_{Q_L} - \lambda_{Q_S}}. \tag{22}$$

[36] The terms in the numerator of (22) (e.g., F^A_E) are shorthand for forcings, have units of W/m^2, and are fundamentally dependent on the choice of A. Generally we will opt to use nonlinear forcings, because they capture the largest nonlinearities in the system, allowing our theory to be useful much further from a reference state than would be true of the completely linear theory. Note that this is directly analogous to the case of global climate sensitivity, where the radiative forcing of a well-mixed greenhouse gas is often nonlinear in its concentration change, but the rest of the sensitivity theory is linear (e.g., feedbacks are assumed constant). A well-known specific example of nonlinear forcing is the approximately logarithmic dependence of radiative forcing on the CO_2 concentration ratio [e.g., *Ramaswamy*, 2001, Table 6.2]. In our case, general expressions for the nonlinear forcings are

$$\begin{aligned}
F^A_{Q_S} &\equiv \int_{A_0}^{A}\left(\frac{\partial Q_S}{\partial A'} - \frac{1}{\rho c_p g_a}\frac{\partial Q_S}{\partial T_S}\frac{\partial H}{\partial A'}\right)dA' \\
F^A_{Q_L} &\equiv \int_{A_0}^{A}\left(\frac{\partial Q_L}{\partial A'} - \frac{1}{\rho c_p g_a}\frac{\partial Q_L}{\partial T_S}\frac{\partial H}{\partial A'}\right)dA' \\
F^A_E &\equiv \int_{A_0}^{A}\left(\frac{\partial E}{\partial A'} - \frac{1}{\rho c_p g_a}\frac{\partial E}{\partial T_S}\frac{\partial H}{\partial A'}\right)dA'.
\end{aligned} \tag{23}$$

[37] Each of these is modified from the direct forcing of a surface flux (e.g., $\int(\partial Q_S/\partial A')dA'$) by an additional term, dependent on $\partial H/\partial A$, that arises because of the dependence of $\mathrm{d}T_S/\mathrm{d}A$ on $\partial H/\partial A$ in (16). This additional term always causes F^A_H to be equal to zero, but in effect transmits the impacts of $\partial H/\partial A$ to the other forcing terms.

[38] The λ terms in the denominator of (22) (e.g., λ_E) represent feedbacks, have units of W/m^2/K, and are independent of the choice of A:

$$\begin{aligned}
\lambda_{Q_S} &\equiv (1+\gamma)\frac{\partial Q_S}{\partial T_S} + \frac{\partial Q_S}{\partial \theta_M} + \xi\frac{\partial Q_S}{\partial q_M} \\
\lambda_{Q_L} &\equiv (1+\gamma)\frac{\partial Q_L}{\partial T_S} + \frac{\partial Q_L}{\partial \theta_M} + \xi\frac{\partial Q_L}{\partial q_M} \\
\lambda_H &\equiv (1+\gamma)\frac{\partial H}{\partial T_S} + \frac{\partial H}{\partial \theta_M} + \xi\frac{\partial H}{\partial q_M} \\
\lambda_E &\equiv (1+\gamma)\frac{\partial E}{\partial T_S} + \frac{\partial E}{\partial \theta_M} + \xi\frac{\partial E}{\partial q_M}.
\end{aligned} \tag{24}$$

[39] Thus, before we choose a specific variable to assign as A, we can generally investigate the feedbacks $\lambda_{Q_S}, \lambda_{Q_L}, \lambda_H$, and λ_E. The sign convention for feedbacks in (22) has anticipated that surface enthalpy fluxes and longwave radiation will act as negative feedbacks, and shortwave radiation will act as a positive feedback (in the absence of cloud radiative effects, λ_{Q_S} will be nearly zero).

[40] If we can solve for all the terms in (22), then we can use (16) to determine changes in T_S, or (20) to

determine changes in q_M. It is also straightforward to then calculate the sensitivity of surface fluxes to changes in A (using (A8)–(A11) and (22)). For example, changes in the latent heat flux (δE) are given generally by $\delta E = F_E^A + \lambda_E \delta\theta_M$; if F_E^A were the only nonzero forcing, then this would simplify to $\delta E = F_E^A \times (\lambda_H + \lambda_{Q_L} - \lambda_{Q_S})/(\lambda_H + \lambda_E + \lambda_{Q_L} - \lambda_{Q_S})$. Though we will not discuss the sensitivity of surface fluxes further, the solutions we will give below for $d\theta_M/dA$ contain all of the terms necessary to calculate surface flux sensitivities to an arbitrary variable.

2.4. Feedbacks: λ_H, λ_E, λ_{Q_S}, and λ_{Q_L}

[41] The enthalpy flux feedbacks are typically most important, and can be simply calculated from our bulk formulae:

$$\lambda_H = \rho c_p g_a \gamma \tag{25}$$

$$\lambda_E = \rho L_v \frac{g_a g_v}{g_a + g_v} \frac{\partial q^*}{\partial T} \left[1 + \gamma - \xi \left(\frac{\partial q^*}{\partial T} \right)^{-1} \right], \tag{26}$$

where $\partial q^*/\partial T$ is considered to be evaluated at the reference state surface temperature. For a relatively moist reference land surface with $g_a = 0.025\mathrm{m/s}, g_v = 0.008\mathrm{m/s}$, with $\gamma \sim 0.2, \xi/(\partial q^*/\partial T) \sim -0.31$ (using the moist-adiabatic approximation for $\xi \approx -c_p/L_v$), and a surface temperature of $\sim 300\mathrm{K}$, $\lambda_H \sim 5.8\mathrm{W/m^2/K}$, and $\lambda_E \sim 34\mathrm{W/m^2/K}$. As we will soon show, this implies that λ_E is generally the dominant feedback for warm and moist land surfaces. Since λ_E decreases as g_v drops, the surface-ML system is typically more sensitive for a dry reference state than a moist one.

[42] In the work of B00, the radiative feedbacks are both assumed to be zero, since the surface net radiation is a prescribed parameter. As we will soon show, this is likely a fine approximation for λ_{Q_L}. However, changes in shortwave forcing associated with changes in cloud properties may be quite important. Despite this potential importance, since we do not have a straightforward physical basis for understanding sensitivities such as $\partial Q_S/\partial q_M$, we will generally take the shortwave radiative feedback λ_{Q_S} to be zero. We will later attempt to empirically evaluate λ_{Q_S} in the two-column model simulations with cloud-radiation interactions enabled.

[43] The longwave flux feedback is typically weak; consider the limit of a ML that is optically thick in most of the infrared, so that we can assume that both surface and ML emit as blackbodies. Then, the net longwave radiation from the surface simply increases with the thermal contrast between the surface and the boundary layer:

$$\lambda_{Q_L} = 4\sigma_B T_{S0}^3 \gamma, \tag{27}$$

where σ_B is the Stefan-Boltzmann constant, and we have linearized the longwave emission from the surface and atmosphere about a reference state surface temperature T_{S0}. For the reference conditions mentioned above, this implies $\lambda_{Q_L} \sim 1.2\mathrm{W/m^2/K}$. As compared to λ_H of 5.8 W/m^2/K and λ_E of 34 W/m^2/K, longwave feedbacks are relatively insignificant.

[44] In the opposite limit of a ML that is optically thin in the IR, as might be the case under much cooler conditions, λ_{Q_L} rises to $4\sigma_B T_{S0}^3(1+\gamma) \approx 5.7\mathrm{W/m^2/K}$ for $T_{S0} = 275\mathrm{K}$. Because λ_E decreases rapidly as surface temperature drops (to $\sim 15\mathrm{W/m^2/K}$ for a 275 K surface and the same assumptions as above), λ_{Q_L} can rise considerably in relative importance for colder situations, but it generally is not the dominant feedback unless λ_H and λ_E are also lowered due to weak reference-state surface winds or low surface roughness.

[45] The study of *Brubaker and Entekhabi* [1996] suggests nearly the same order of importance of feedbacks as we have estimated here, though the differences in their model structure as compared to ours translates to different analytic feedback expressions, and the magnitude of their turbulent feedbacks is generally weaker, because their effective value of g_a is only 0.004 for forced turbulent enthalpy fluxes (as opposed to our $g_a = 0.025$). As a result of the relative weakness of turbulent transfer, and the lower infrared optical thickness of the ML, radiation may be a slightly stronger negative feedback in their results than sensible heat fluxes. They also include a free-convective enhancement of turbulent enthalpy fluxes that depends on the buoyancy velocity scale, with the result that additional feedbacks emerge beyond what we have discussed. The most significant common finding between our study and the work of *Brubaker and Entekhabi* [1996] is the strong negative temperature feedback on soil temperatures due to the dependence of evaporation on the saturation specific humidity at the surface (strength ~ 12.66 W/m^2/K in their work); this mechanism is included in our evaporative feedback λ_E.

2.5. Forcing by Surface Conductance to Water Vapor ($A \rightarrow g_v$)

[46] We will now demonstrate how the theory applies to three specific cases of A. First, we consider $A \rightarrow g_v$, the bulk surface conductance to water vapor. In this case, Q_S, Q_L, and H do not depend explicitly on g_v, so the only nonzero forcing in the numerator of (22) is $F_E^A \rightarrow F_E^{g_v}$. Furthermore, since $\partial H/\partial g_v = 0, F_E^{g_v}$ contains only the contribution from $\partial E/\partial g_v = g_a E_0/(g_v(g_a + g_v))$, where E_0 is the reference-state latent heat flux:

$$F_E^{g_v} = \int_{g_{v0}}^{g_v} \frac{g_a E_0}{g_v'(g_a + g_v')} dg_v'. \tag{28}$$

[47] If the latent heat flux varies much more slowly than g_v itself, then we can assume E_0 is a constant, and the integrated forcing is given by

$$F_E^{g_v} = E_0 \ln\left(\frac{g_v}{g_{v0}} \frac{g_a + g_{v0}}{g_a + g_v} \right). \tag{29}$$

[48] Plugging (29) into (22) and (16), and dropping λ_{Q_S} for brevity, we have

$$\delta\theta_M = \frac{-E_0}{\lambda_{Q_L}+\lambda_H+\lambda_E}\ln\left(\frac{g_v}{g_{v0}}\frac{g_a+g_{v0}}{g_a+g_v}\right) \tag{30}$$

$$\delta T_S = (1+\gamma)\delta\theta_M. \tag{31}$$

[49] We see that reducing g_v leads to warming of the surface and boundary layer, in direct proportion to changes in the logarithm of the evaporative efficiency $\beta = g_v/(g_a+g_v)$ (8). A boundary layer warming scale in response to a reduction in surface conductance to water vapor is given by the quantity $\Theta_{g_v} \equiv E_0/(\lambda_{Q_L}+\lambda_H+\lambda_E)$. For the aforementioned reference parameters, which pertain to a moist surface at warm temperatures, and a reference state latent heat flux of $E_0 \sim 120\mathrm{W/m^2}$, this gives a warming scale of $\Theta_{g_v} \sim 2.9\mathrm{K}$. Thus, we expect a 10% change in β to result in a temperature change of $\sim$0.29 K.

2.6. Forcing by Surface Albedo ($A \rightarrow \alpha$)

[50] The forcing for albedo changes is even more straightforward, since as in the case of g_v, three of the four terms in the surface energy budget (Q_L, H, and E) do not depend explicitly on the albedo, and thus the only nonzero forcing in the numerator of (22) is $F^A_{Q_S} \rightarrow F^\alpha_{Q_S}$. Furthermore, the forcing in this case is linear in albedo changes. The surface net shortwave radiation is given by $Q_S = (1-\alpha)Q_S^\downarrow$, so

$$F^\alpha_{Q_S} = \int_{\alpha_0}^{\alpha}\frac{\partial Q_S}{\partial \alpha'}d\alpha' = -Q_S^\downarrow(\alpha-\alpha_0) = -\frac{Q_{S0}}{1-\alpha_0}\delta\alpha, \tag{32}$$

where Q_{S0} and α_0 are the reference state net surface shortwave radiation and albedo, respectively, and we have used $\alpha-\alpha_0 \equiv \delta\alpha$. As in section 2.5, we can plug (32) into (22) and (16), and we obtain

$$\delta\theta_M = \frac{-Q_{S0}/(1-\alpha_0)}{\lambda_{Q_L}+\lambda_H+\lambda_E}\delta\alpha \tag{33}$$

$$\delta T_S = (1+\gamma)\delta\theta_M. \tag{34}$$

[51] Increasing albedo thus leads to cooling, and decreasing albedo leads to warming. If we assume $\alpha_0 \sim 0.2$ and $Q_{S0} \sim 200\mathrm{W/m^2}$, then a large change in albedo of $\delta\alpha \sim 0.1$ would lead to a temperature change of only $\sim$0.6 K.

2.7. Forcing by Surface Aerodynamic Conductance ($A \rightarrow g_a$)

[52] Consideration of the case where $A \rightarrow g_a$ is considerably more complex, since E depends explicitly on g_a, and the explicit dependence of H on g_a further suggests that $F^{g_a}_{Q_S}$ and $F^{g_a}_{Q_L}$ may be nonzero. First, we note that

$$\frac{\partial H}{\partial g_a} = \rho c_p(T_{S0}-\theta_{M0}) = \frac{H_0}{g_a}, \tag{35}$$

where H_0 is the reference state sensible heat flux. Taking $\partial Q_S/\partial T_S = 0$ implies that $F^{g_a}_{Q_S} = 0$; Q_L does not depend explicitly on g_a, but since $\partial Q_L/\partial T_S$ is nonzero, we find that

$$\begin{aligned} F^{g_a}_{Q_L} &= \int_{g_{a0}}^{g_a} -\frac{4\sigma_B T_{S0}^3 H_0}{\rho c_p g_a'^2}dg_a' \\ &= \frac{4\sigma_B T_{S0}^3 H_0}{\rho c_p}\left(\frac{1}{g_a}-\frac{1}{g_{a0}}\right). \end{aligned} \tag{36}$$

[53] The forcing of latent heat flux by changes in g_a has contributions from both the explicit dependence of E on g_a, and the part of $F^{g_a}_E$ that depends on $\partial H/\partial g_a$:

$$\begin{aligned} F^{g_a}_E &= \int_{g_{a0}}^{g_a}\left(\frac{\partial E}{\partial g_a'}-\frac{1}{\rho c_p g_a'}\frac{\partial E}{\partial T_S}\frac{H_0}{g_a'}\right)dg_a' \\ &= \int_{g_{a0}}^{g_a}\left[\rho L_v\frac{g_v^2(q^*(T_{s0})-q_{b0})}{(g_a'+g_v)^2}-\frac{\rho L_v\dfrac{g_v g_a'}{g_a'+g_v}\dfrac{\partial q^*}{\partial T}H_0}{\rho c_p g_a'^2}\right]dg_a' \\ &= \int_{g_{a0}}^{g_a}\frac{g_v}{g_a'(g_a'+g_v)}\left(E_0-\frac{H_0}{B_e}\right)dg_a' \\ &= \left(E_0-\frac{H_0}{B_e}\right)\ln\left(\frac{g_a}{g_{a0}}\frac{g_{a0}+g_v}{g_a+g_v}\right), \end{aligned} \tag{37}$$

where B_e is the equilibrium Bowen ratio [e.g., *Hartmann*, 1994]:

$$B_e = \frac{c_p}{L_v\frac{\partial q^*}{\partial T}}. \tag{38}$$

[54] To obtain surface temperature changes, we must also integrate the portion of (16) that depends directly on $\partial H/\partial A$. Putting the results of (36) and (37) into (22) and (16), and performing this extra integration for δT_S, we obtain

$$\delta\theta_M = \frac{-\left(E_0-\frac{H_0}{B_e}\right)\ln\left(\frac{g_a}{g_{a0}}\frac{g_{a0}+g_v}{g_a+g_v}\right)-\frac{4\sigma_B T_{S0}^3 H_0}{\rho c_p}\left(\frac{1}{g_a}-\frac{1}{g_{a0}}\right)}{\lambda_{Q_L}+\lambda_H+\lambda_E} \tag{39}$$

$$\delta T_S = \frac{H_0}{\rho c_p}\left(\frac{1}{g_a}-\frac{1}{g_{a0}}\right)+(1+\gamma)\delta\theta_M. \tag{40}$$

[55] The sensitivity expressions in this case are more complex than in the cases of changes in albedo and surface conductance to water vapor—the sign of $\delta\theta_M/\delta g_a$ is ambiguous, and δT_S is not simply related to $\delta\theta_M$ by the multiplicative factor $(1+\gamma)$. Because terms in the numerator of (39) have opposing signs, changes in θ_M due to changes in g_a are typically small; the largest changes in temperature are often associated with the term $H_0/(\rho c_p)(g_a^{-1}-g_{a0}^{-1})$ in the expression for δT_S. If the aerodynamic conductance is halved from a normal value of 0.025 m/s to 0.0125 m/s, and the reference-state

sensible heat flux is 20 W/m^2, then θ_M would increase by ~0.25 K, but T_S would rise by a much larger ~1 K.

3. Comparison With B00 Results

[56] The first question we should ask of this theory is: does it reasonably approximate the sensitivities obtained with the full set of equations from B00? To answer this question, we have written a MATLAB script to numerically solve the full set of equations from B00, available at: http://mit.edu/~twcronin/www/code/Betts2000_EBLmodel.m. Our solutions reproduce the results from B00 to within 0.01 K and 0.01 g/kg (Betts, 2013, personal communication), and we can compare the theoretical sensitivities to the numerical solutions for all three choices of forcing parameter, $A \rightarrow (g_v, \alpha, g_a)$. B00 does not explicitly use an albedo in his equations, but by assuming a fixed Q_L of 50 W/m^2, and a surface albedo of 0.2, his default surface net radiation Q^* of 150 W/m^2 implies $Q_S^{\downarrow}$=250W/m^2, enabling us to define the forcing $F_{Q_S}^{\alpha}$ from (32). We obtain sensitivities by comparing reference state and perturbation solutions with g_v and g_a varied by factors of 1.1^n, where $n=\pm(1, 2, 3, \ldots, 9, 10)$, and α modified by $\pm(5, 10, 15, \ldots, 45, 50)\%$. Reference-state values are g_{v0}=0.008m/s, α_0=0.2, and g_{a0}=0.025m/s. The range of g_v spanned is 0.0031 to 0.0207 m/s, which corresponds to most of the range of values covered in B00.

[57] Figure 2 shows a comparison of our theory with the solutions to the full equations from B00, using the reference state parameters from Table 1 of B00 (also see the "normal values" column of Table 3). We see that the sensitivity theory with linear forcings (dot-dashed lines in Figure 2; equation A16) is accurate only very close to the reference state for $\pm g_v$ and $\pm g_a$ perturbations, and that the usage of nonlinear forcings (solid lines in Figure 2; see Table 2) significantly extends the validity of the theory. Note that the shortwave forcing due to albedo changes is linear in α, so there is no difference between linear and nonlinear forcings. In the model of B00 at least, the dominant nonlinearity in the sensitivity of temperature to g_v or g_a is due to nonlinear forcing of the surface energy budget by changing g_v or g_a, rather than nonconstancy of the feedbacks. As noted above, the importance of nonlinear forcing is directly analogous to the problem of climate sensitivity, where radiative forcing from greenhouse gases is generally a nonlinear function of concentration changes; it even turns out that the evaporative forcing due to changing g_v is logarithmic in the ratio of evaporative efficiencies β/β_0, just as the radiative forcing due to changing CO_2 is approximately logarithmic in the ratio of final to initial CO_2 concentrations.

[58] To assure that the theory compares well with the B00 model across a range of reference states, and not merely the one shown in Figure 2, we can plot the theoretical temperature change ordinates against the B00 model temperature change abscissas, for many reference states. In such a plot, collapse onto the 1-1 line would indicate robustness of the theory across the full set of reference states tested. Figure 3 shows that such collapse indeed occurs; for each of the 20 different reference states described in Table 3, the theory very nearly matches the changes in temperature given by numerical solutions to the full equation set of B00. Once again, the use of nonlinear forcings vastly improves the fidelity of the theory to its parent model, especially for large perturbations to g_v and g_a; hereafter, we will show comparisons only using the nonlinear-forcing theory.

4. Two-Column Radiative-Convective Model Simulations

4.1. Model Setup

[59] To further evaluate the theory described in section 2, we use a two-column radiative convective (RC) model, which is described in *Abbot and Emanuel* [2007];

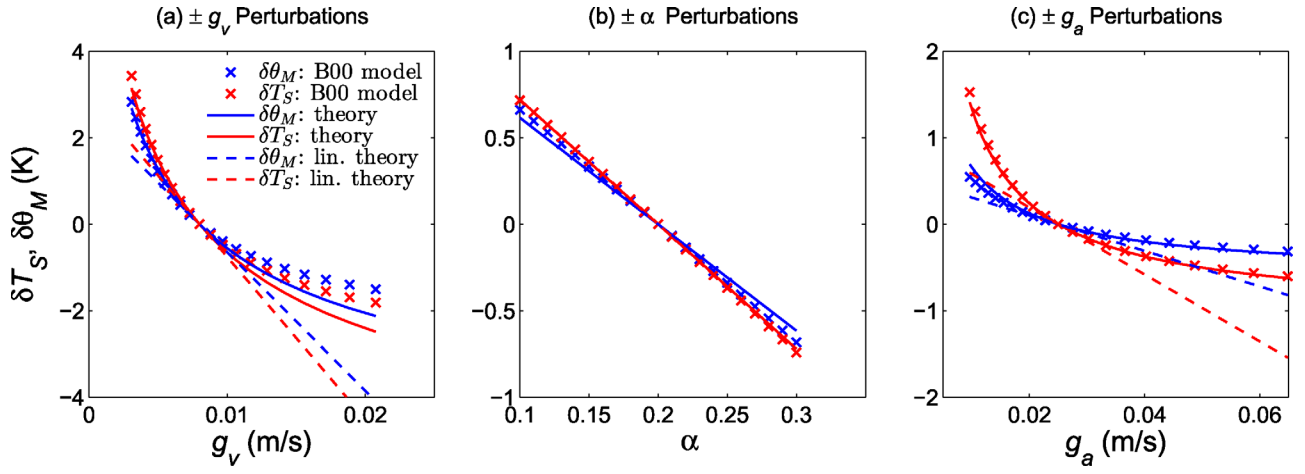

Figure 2. Comparison of changes in surface temperature (δT_S, red) and ML potential temperature ($\delta\theta_M$, blue) for the theory (solid and dashed lines) and full numerical solutions from the B00 model ("x"-symbols), for perturbations in individual surface parameters (a) $\pm g_v$, (b) $\pm\alpha$, and (c) $\pm g_a$. Theoretical values of δT_S and $\delta\theta_M$ and are calculated using the fully nonlinear forcing expressions based on (23) (solid lines) and using the linear forcing expressions of (A15) (dashed lines).

Table 3. Reference-State Parameters Used in Comparison of Theory and Solutions to Full Equation Set of B00 (Figure 3)[a]

Parameter	Normal Value	Alternate Values	Units
Stability, Γ	0.06	0.04,0.05,0.07	K/hPa
Subsaturation just above ML, $\mathcal{P}_\mathcal{T}$	100	60,140	hPa
Surface net radiation, $\overline{Q^*}$	150	110,130,170	W/m^2
Radiative cooling rate, $\overline{Q_R}$	3	1,2	K/day
Evaporative cooling rate, $\overline{Q_C}$	0	1,2,3	K/day
Potential temperature at 940 hPa, θ_{00}	303	283,288,293,298,308,313	K

[a]Aside from the reference state that uses the normal value for all parameters, each of 19 other reference states is calculated by varying one of the six parameters ($\Gamma, \mathcal{P}_\mathcal{T}, \overline{Q^*}, \overline{Q_R}, \overline{Q_C}$, or θ_{00}) to one of the alternate values listed below, while holding the other five parameters fixed at normal values. Alternate values of all parameters but θ_{00} are taken from B00 (see Table 1 of B00).

a schematic of the model is shown in Figure 4. The model uses the convection scheme of *Emanuel and Zivkovic-Rothman* [1999] and the cloud scheme of *Bony and Emanuel* [2001]. In all simulations, the model has one column over land and a second column over ocean. In an attempt to ensure that the free-tropospheric temperatures do not change very much as a land surface parameter is varied, we perform simulations with fixed SST in the ocean column. Together with nonrotating dynamics, the fixed SST lower boundary strongly constrains the average tropospheric temperature profile of both columns, approximately enforcing the key assumption of equation (12). Lateral boundary conditions are periodic, so that air exiting the land column in either direction enters the ocean column, and the system is not subjected to any time-varying large-scale forcing. For all simulations, we use a CO_2 concentration of 360 ppm, and a fixed solar zenith angle whose cosine is 2/3 (equal to the planetary-average, insolation-weighted value); all but one set of simulations are performed with no diurnal cycle of solar radiation.

[60] We perform simulations with and without interactions between clouds and the radiation scheme. We use a relatively fine vertical resolution of 10 hPa, and a short timestep of 1 min, but horizontal resolution is extremely coarse, with column widths of 4000 km. The intent of such wide columns is to ensure the weakness of horizontal advective tendencies—this only breaks down if the land is extremely dry and warm. Simulations are typically spun up for 100 days, and then run to collect data for additional 100 days.

[61] The land surface parameters that we vary are the bulk surface conductance to water vapor, g_v, the surface albedo, α, and the bulk aerodynamic conductance over land, g_a. We actually modify g_a by varying c_k, and using a fixed value of $|\mathbf{v_s}|$ within each set of reference plus perturbation simulations, so that $\delta g_a/g_{a0} = \delta c_k/c_{k0}$ (see equation (7)). We use the background oceanic drag

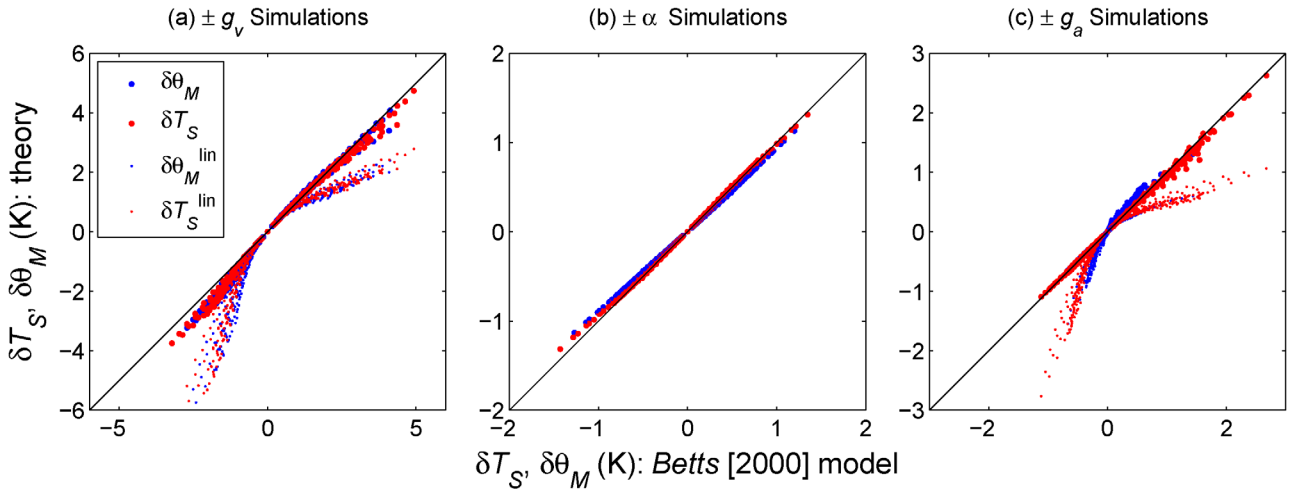

Figure 3. Comparison of changes in surface temperature (δT_S, red) and ML potential temperature ($\delta\theta_M$, blue) for the theory and full numerical solutions from B00, for perturbations of individual land surface parameters (a) $\pm g_v$, (b) $\pm\alpha$, and (c) $\pm g_a$. Changes in surface temperature δT_S and boundary layer potential temperature $\delta\theta_M$ are computed from the full equation set of B00 (abscissas) and based on the theory of section 2 (ordinates). Theoretical values of $\delta\theta_M$ and δT_S are calculated using the fully nonlinear forcing expressions based on (23) (large solid points) and using the linear forcing expressions of (A15) (small points). A 1-1 line is drawn in black on each subfigure for reference, and each subfigure includes points from 20 reference states, each with 20 perturbations to g_v,α, or g_a—see text and Table 3 for details.

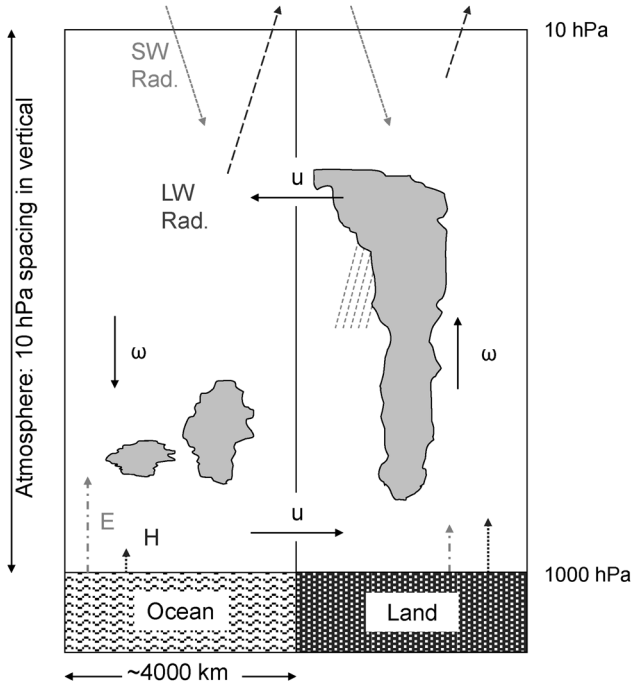

Figure 4. Schematic of two-column radiative-convective (RC) model used in this study, described in *Abbot and Emanuel* [2007] and *Nilsson and Emanuel* [1999]. Dynamics of the overturning circulation are determined by solving prognostic vorticity equations in the direction orthogonal to the model domain.

coefficient $c_{D0}=0.0015(\neq c_k)$ for calculating surface stresses, which act to dissipate overturning circulations.

4.2. Reference Simulations

[62] A particular reference state has two separable components: the choice of land surface parameters $(g_{v0}, \alpha_0, c_{k0})$ and the choice of atmospheric boundary conditions. In the radiative-convective model, it is no longer possible to directly impose values for any of the six reference-state parameters that were externally specified in section 3 (these parameters were described in Table 3). For the radiative-convective model, we will use three external atmospheric boundary conditions: the surface windspeed for enthalpy fluxes $|\mathbf{v_s}|$ (units: m/s), the surface temperature in ocean column T_{SS} (units: K), and the top-of atmosphere insolation I_{TOA} (units: W/m^2).

[63] Due to the absence of well-studied reference surfaces for many vegetation types, we will focus our attention on a single reference surface, with $g_{v0}=0.008\mathrm{m/s}$, $\alpha_0=0.23$, and $c_{k0}=0.0048$. These parameters are based on the reference grass surface described by *Allen et al.* [1998] in UN FAO working paper 56. Since the *Allen et al.* [1998] surface is typically used to calculate a reference evapotranspiration for the purpose of estimating crop water requirements, it has a value of g_v near the upper range of observations for real land surfaces (0.0143 m/s). In order to span a broader range of realistic conditions, we use a somewhat reduced value of gv_0, but the same values of α and c_k as in *Allen et al.* [1998] (the value of c_k is derived from Box 4 of *Allen et al.* [1998], assuming that surface enthalpy flux bulk formulae use the 2 m wind speed).

Table 4. Atmospheric Boundary Conditions Used in Two-Column RC Model Simulations

	Parameter, Units		
Simulation	$\lvert\mathbf{v_s}\rvert$ (m/s)	T_{SS} (°C)	I_{TOA} (W/m^2)
Standard	5.0	28.0	400.0
V−−	1.5	32.0	400.0
V−	2.5	28.0	400.0
V+	10.0	28.0	400.0
V++	15.0	28.0	400.0
T−−−	5.0	4.0	280.0
T−−	5.0	16.0	320.0
T−	5.0	24.0	360.0
T+	5.0	32.0	420.0
T++	5.0	40.0	440.0

[64] For our reference surface parameters, we perform 10 sets of sensitivity experiments with a broad range of combinations of the three external atmospheric parameters $|\mathbf{v_s}|$, T_{SS}, and I_{TOA} (see Table 4 for details). In all but one set of simulations, we do not include the radiative effects of clouds in model calculations, as the convective parameterization produces mostly high clouds, which do not have much effect on the results, but require longer simulations to attain clean results, due to the greater variability of simulations with interactive clouds.

4.3. Perturbation Simulations

[65] For each reference simulation, we test the theory by performing simulations with perturbations to g_v, α, and c_k. As in section 3, we vary g_v and c_k by factors of 1.1^n, where $n=\pm(1,2,3,\ldots,9,10)$, and we vary α by $\pm(5,10,15,\ldots,45,50)\%$. Our perturbation simulations thus span a very broad range of g_v and c_k (0.0031–0.0207 m/s, and 0.0019–0.0124, respectively), and most of the range of α observed for nonsnowy land surfaces (0.115–0.345). We compute forcing and feedback terms near each reference state (based on reference-state fluxes, temperatures, and boundary layer cooling rates), and then compare simulated changes in surface temperature δT_S and boundary layer potential temperature $\delta\theta_M$ to the predictions of the theory from section 2. Results in all figures show simulated changes δT_S and $\delta\theta_M$ for the land column only.

[66] To provide a quantitative figure of merit, we also define the R^2 for a variable X as

$$R^2(X)=1-\frac{\Sigma\left(X_{\mathrm{model}}-X_{\mathrm{theory}}\right)^2}{\Sigma\left(X_{\mathrm{model}}-\overline{X_{\mathrm{model}}}\right)^2}, \qquad (41)$$

i.e., as unity minus the fraction of the model variance that remains after comparison with the theory. Note that this is the value of R^2 conditioned on the assumption that $X_{\mathrm{model}}=X_{\mathrm{theory}}$, and not based on a best linear fit ($X_{\mathrm{model}}=mX_{\mathrm{theory}}+b$). Values of R^2 are shown in the corresponding figures.

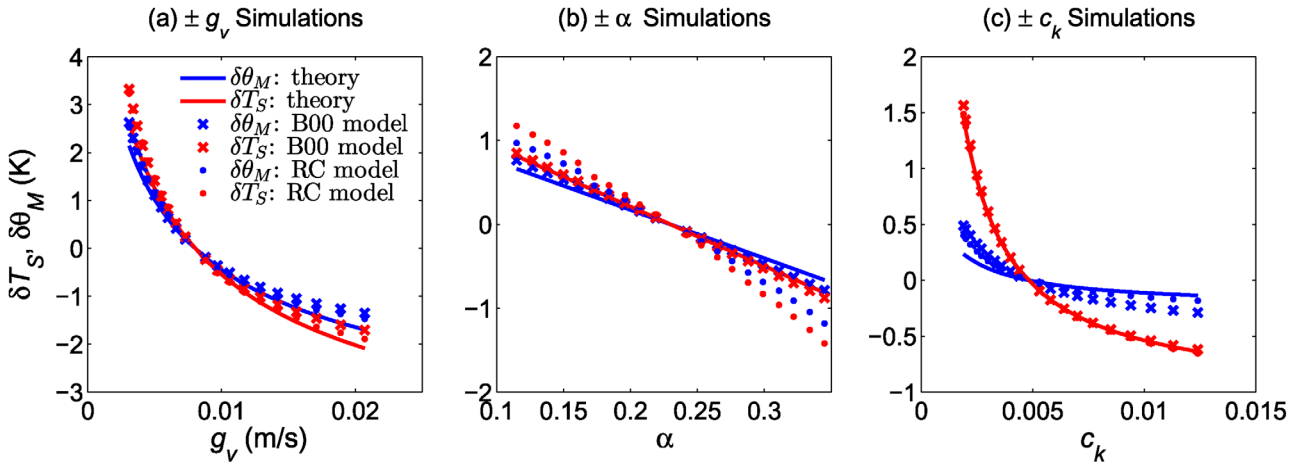

Figure 5. Comparison of changes in surface temperature (δT_S, red) and ML potential temperature ($\delta\theta_M$, blue) for the theory (solid lines), RC model simulations (filled circles), and full numerical solutions from the B00 model (x-symbols). Subfigures show results for perturbations of individual surface parameters (a) $\pm g_v$, (b) $\pm\alpha$, and (c) $\pm c_k$. All of the reference-state parameters for the sensitivity theory and the B00 model are calculated from the RC model simulation using the "Standard" atmospheric boundary conditions from Table 4.

4.4. Results

[67] We first discuss the three-way comparison of the RC model results with both the predictions of the theory and the numerical solutions to the full equations from B00, for the case of no cloud-radiation interactions, and the "Standard" set of atmospheric boundary conditions from Table 4. Figure 5 shows that RC model simulations where g_v or c_k are varied (Figures 5a and 5c, respectively) support the theory quite well; RC model results also compare well with the B00 model results for these surface parameters. Both the theory and the B00 model have less skill with albedo variations (Figure 5b); though the functional form of temperature changes as a function of albedo is correctly predicted to be nearly linear, the theory and B00 model results significantly underestimate changes in temperature produced by the RC model simulations. The reasons for this underestimation will soon be discussed in detail. Figure 5 also shows that in general, the solutions to the full set of equations from B00 are a slightly better fit to the RC model results than is the analytic theory. This is especially evident at low values of g_v (Figure 5a), all values of albedo (Figure 5b), and low values of c_k (Figure 5c). The better match between the B00 model results and the RC model results at low values of g_v, where temperatures increase more rapidly than the theory predicts, is likely due to reduction in the evaporative feedback λ_E, which the theory assumes to be a constant.

[68] Similar to section 3, we test robustness of the theory across the range of reference states described in Table 4, by plotting theoretical temperature change ordinates against RC model temperature change abscissas, with a perfect fit reflected by collapse onto the 1-1 line. Such collapse nearly occurs for $\pm g_v$ and $\pm c_k$ perturbation simulations, where the theory explains from 83%–99% of the deviations in both T_S and θ_M from the reference state (Figures 6a and 6c). The theory has less skill with albedo variations; as in the "Standard" reference state result shown in Figure 5b, the theory tends to underestimate the magnitude of warming or cooling produced by the RC model (Figure 6b). However, even for $\pm\alpha$ simulations, the theory still captures between over 70% of the RC model variance in $\delta\theta_M$ and δT_S.

[69] The lower skill of the theory for $\pm\alpha$ simulations, as compared to $\pm(g_v, c_k)$ simulations, is largely due to the violation of constant free-tropospheric temperatures (equation (12)). As in the real tropics, the nonrotating dynamics in our RC model allow only very weak horizontal temperature gradients above the boundary layer [*Sobel et al.*, 2001]. This dynamical constraint on temperature gradients, together with the fixed-SST lower boundary in the ocean column, strongly constrains the free-tropospheric thermal profile in both columns. With only one buffering ocean column, however, the large changes in convection over land due to changes in albedo can significantly impact the modeled thermal structure above the well-mixed boundary layer. For simulations where α is varied, changes in θ at 700 hPa ($\delta\theta_{700\text{hPa}}$) are of the same magnitude as, and well-correlated with, changes in θ_M (Figure 7). This is consistent with a two-column RC model sensitivity $|d\theta_M/d\alpha|$ that is greater than the theory would predict, as is generally the case in our results (Figures 5b and 6b). We would expect the addition of more buffering ocean columns in the RC model to decrease the sensitivity of free-tropospheric temperatures to albedo, and thus improve the agreement between RC model results and theory. For simulations where g_v or c_k are varied, Figure 7 shows that changes in free-tropospheric potential temperature ($\delta\theta_{700\text{hPa}}$) are small and relatively uncorrelated with changes in boundary layer potential temperature ($\delta\theta_M$), so the assumption of (12) is roughly valid; changes in the thermal structure of the lower free troposphere may merely add noise to our results.

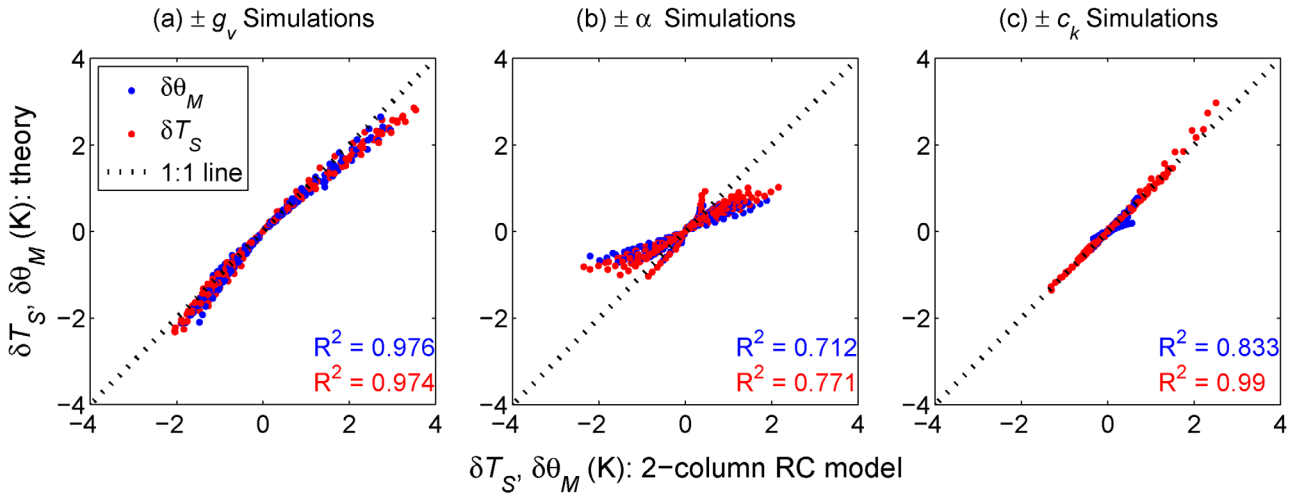

Figure 6. Comparison of changes in surface temperature (δT_S, red) and ML potential temperature ($\delta\theta_M$, blue) for the theory, and the $\pm(g_v, \alpha, c_k)$ perturbation simulations with the RC model, for the 10 atmospheric boundary conditions listed in Table 4. Subfigures show results for perturbations of individual surface parameters (a) $\pm g_v$, (b) $\pm\alpha$, and (c) $\pm c_k$, as described in the text. Values of R^2 as defined in equation (41) are indicated in text for the model-theory comparison for $\delta\theta_M$ (blue) and δT_S (red).

[70] We can also use RC model simulation results to attempt to assess the importance of cloud-radiation interactions, as well as the diurnal cycle, for the validity of the theory; we will assess each of these effects separately for a single reference state corresponding to the "Standard" set of atmospheric boundary conditions.

[71] We find that longer RC model simulations are generally needed to obtain clean results when cloud-radiation interactions are enabled. To obtain the results shown in Figure 8, data were collected over 800 days of model time (rather than 100). Generally speaking, the theory still captures a great deal of the behavior of RC model results, especially for simulations where g_v is perturbed. Departure from good fits in the $\pm\alpha$ and $\pm c_k$ simulations seems to reveal aspects of unexpected behavior in the RC model, rather than illuminating deficiencies in the theory. Cloud-radiation interactions introduce random noise, as well as systematic changes, to the RC model simulations, and sometimes these systematic changes can occur abruptly as the land surface parameter is varied. For example, the abrupt deviation of the RC model results from the predictions of the theory as c_k is increased past about 0.007 coincides with an abrupt change in surface net shortwave radiation, by about 5 W/m^2. The large drop in temperatures at the highest value of albedo coincides with an abrupt decrease in the sensible heat flux by about 7 W/m^2, and a drop in the LCL by over 15 hPa, as compared to results at the next-highest albedo value. We believe that such behavior is artificial and perhaps represents a constraint of discretization (important transition levels like the tropopause, ML-top, or top of a cloud layer, are sometimes forced to change in discrete jumps), especially with a model that has a limited number of degrees of freedom (i.e., only two columns) and no external sources of variability. Regardless of whether they are physical or not, abrupt changes are not anticipated by our sensitivity theory, and consequently the RC model results are fit less well by the theory when cloud-radiation interactions are enabled. From the standpoint of the sensitivity theory, the principal effects of cloud-radiation interactions are to slightly reduce the reference-state values of Q_{S0} and E_0 due to cloud shading of the surface, and to introduce λ_{Qs} as a small feedback in the denominator of (22). We will discuss the importance of cloud feedbacks in section 5.2.

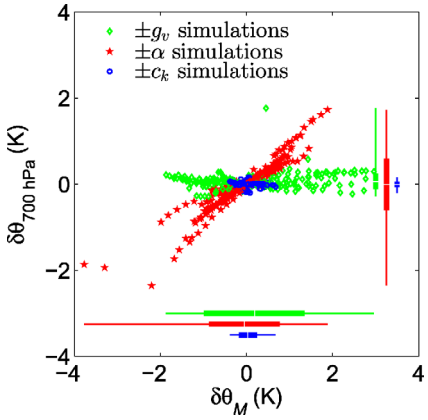

Figure 7. Scatterplot of changes in boundary layer and free-tropospheric potential temperatures, $\delta\theta_M$ and $\delta\theta_{700\text{hPa}}$, in the RC model simulations. Significant changes in free-tropospheric potential temperature ($\delta\theta_{700\text{hPa}}$) violate the assumption of (12) for $\pm\alpha$ simulations. Thick lines indicate $\pm$ 1 standard deviation from the mean, thin lines indicate the range of the data, and white hashes indicate means.

[72] To look at the impacts of the diurnal cycle, we perform RC model simulations with time-varying solar radiation corresponding to a perpetual spring equinox

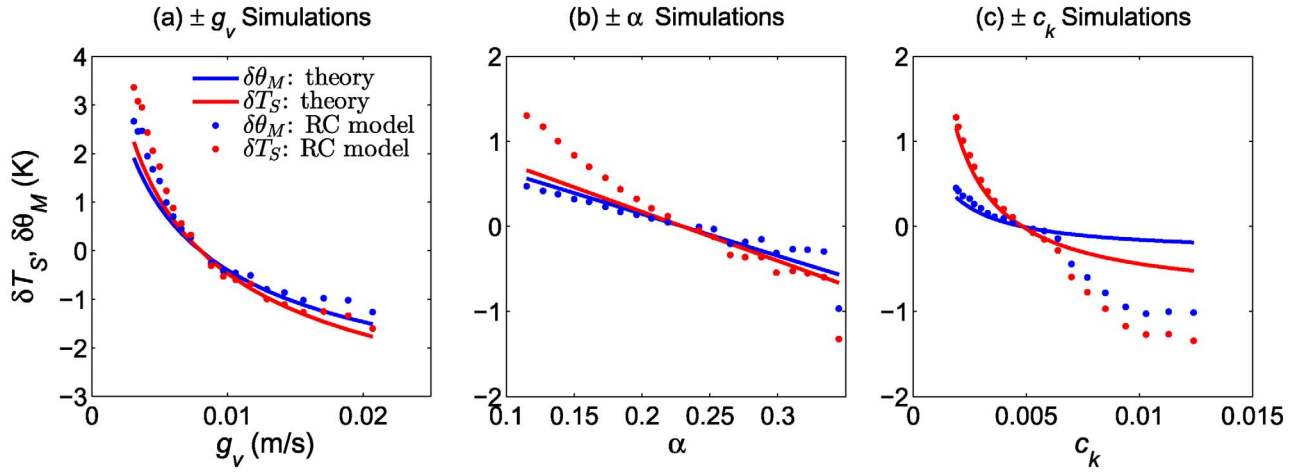

Figure 8. As in Figure 5, but using RC model simulations with cloud-radiation interactions enabled (and no comparison with B00 model). Subfigures are for perturbations of individual surface parameters (a) $\pm g_v$, (b) $\pm\alpha$, and (c) $\pm c_k$.

on the equator, with a slightly reduced value of the solar constant (1256.64 W/m^2) to give a time-mean insolation comparable to the 400 W/m^2 "Standard" choice in Table 4. The land surface is treated as a slab with a heat capacity of 2.1×10^5J/m^2/K, which is slightly lower than the $\sim3\times10^5$J/m^2/K soil heat capacity in *Brubaker and Entekhabi* [1995]. In the reference state, the diurnal cycle of surface temperatures has a maximum of ~37.5°C, a minimum of ~23.5°C, and a time-mean of 29.2°C, which is slightly lower than the 29.6°C in the comparable reference simulation that uses diurnally averaged radiation. The RC model does not have a stable boundary layer parameterization—some discrete number of model levels always is well mixed by hard dry adjustment. The ML depth (P_M, given by the number of dry-adjusted levels) varies between a minimum of 10 hPa at night (1 level) to a maximum of 100 hPa during the early afternoon (10 levels), with gradual growth in the morning and a rapid collapse in the evening. Figure 9 shows that the theory is still somewhat successful at predicting the sensitivity of time-mean temperatures from RC model simulations with a diurnally varying boundary layer. The fit is strikingly good for $\pm g_v$ simulations, suffers from similar issues of sensitivity underestimation for $\pm\alpha$ simulations, and is markedly poorer for $\pm c_k$ simulations. The degradation of the fit for $\pm c_k$ simulations, for both θ_M and T_S, is likely related to the large changes in sensible heat flux that occur, and the assumption of small changes in H that went into the derivation of (39) and (40). From the lowest to the highest values of c_k, H varies from 30.6 to 50.2 W/m^2; these changes are too large to be neglected without consequence, and they are much larger than the changes in H that occur in simulations with diurnally averaged radiation. This raises the question of how the $\pm g_v$ simulations can be so well captured by the theory, when E varies across the range of g_v perturbation simulations by an even larger amount. The answer to this

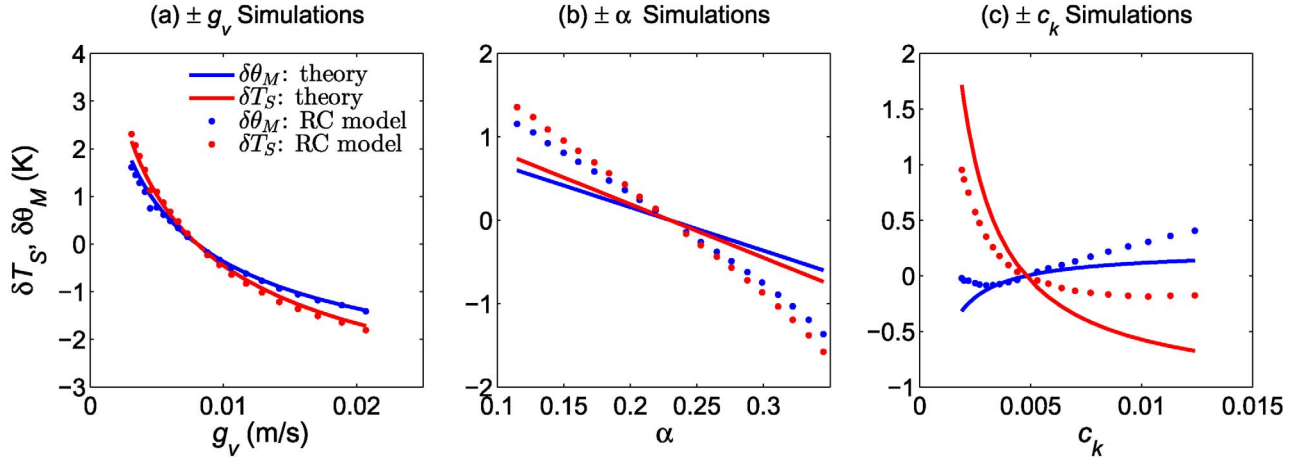

Figure 9. As in Figure 5, but using RC model simulations with a diurnal cycle of insolation (and no comparison to the B00 model). Subfigures are for perturbations of individual surface parameters (a) $\pm g_v$, (b) $\pm\alpha$, and (c) $\pm c_k$, as described in the text. See text for details on the diurnal cycle.

question likely lies in the covariance of E and λ_E, which makes the term $E/(\lambda_H+\lambda_E+\lambda_{Q_L})$ more constant than either its numerator or denominator.

5. Discussion

[73] We believe that the results from sections 3 and 4 generally show the theory to be a useful tool by which to understand the sensitivity of the equilibrium boundary layer over land. However, it is worth taking a step back to discuss some of the important limitations and open questions that relate to the applicability of our results.

5.1. Limitations of the Theory

[74] Neglect of horizontal advection is a major limitation of the theory, and restricts our attention to regions that are large enough in spatial scale, and weak enough in horizontal gradients, for horizontal advective tendencies to be unimportant in the ML. *Brubaker and Entekhabi* [1995] suggest that thermal advection may be unimportant for regions with roughly homogeneous surface conditions that span areas of $\sim 10^4$ to 10^5 km^2, though horizontal moisture advection is always required to balance the water budget in their model. To the extent that the flow in a thermally driven, linearly damped low-level circulation scales with the temperature gradient [e.g., *Nilsson and Emanuel*, 1999, Section 3c], such circulations generate an advective cooling tendency that scales as the square of the temperature gradient. Thus, if ML temperature gradients in the reference state are weak, a linear sensitivity analysis should ignore changes in horizontal advective cooling as a higher-order term—$(\delta\theta_M)^2$—in the ML thermal balance. An interesting subject for future work would be to study how the ML response scales with the horizontal scale of the forcing, which would be relevant for understanding the applicability of the theory to real-world changes in land surface properties.

[75] Another significant limitation, as alluded to above, is the oversimplified treatment of the sensitivity of ML thermal balance involved in deriving (14). A full treatment of the change in ML thermal balance requires differentiation of the total ML cooling $(P_M\overline{Q_\Sigma})$:

$$\frac{d}{dA}\left(P_M\overline{Q_\Sigma}\right)=\left(\overline{Q_{R0}}+\overline{Q_{C0}}\right)\frac{dP_M}{dA}+P_{M0}\left(\frac{d\overline{Q_R}}{dA}+\frac{d\overline{Q_C}}{dA}\right). \tag{42}$$

[76] We can quantify the relative importance of changes in ML thickness versus ML average cooling rates by looking at the logarithmic derivative of (42):

$$\frac{d}{dA}\ln\left(P_M\overline{Q_\Sigma}\right)=P_{M0}^{-1}\frac{dP_M}{dA}+\overline{Q_{\Sigma0}}^{-1}\frac{d\overline{Q_R}}{dA}+\overline{Q_{\Sigma0}}^{-1}\frac{d\overline{Q_C}}{dA} \tag{43}$$

[77] We plot the three terms on the RHS of (43) against changes in θ_M across the full set of simulations to diagnose their relative importances (Figure 10). In general, radiative cooling $(\overline{Q_R})$ decreases with increasing temperature, and convective cooling $(\overline{Q_C})$ increases with increasing temperature, but their relative rates of change per degree of boundary layer warming differ among forcings. The decrease in radiative cooling (the $\overline{Q_R}/\overline{Q_{\Sigma0}}$ term) with increasing θ_M is consistent with increased heating of the ML by surface longwave radiation, which increases more rapidly than downward longwave radiation from the ML itself, because the surface warms more than the ML does. This is particularly important in the case of $\pm c_k$ simulations, where the surface warms much more than the ML, strongly decreasing the average radiative cooling rate of the ML. The

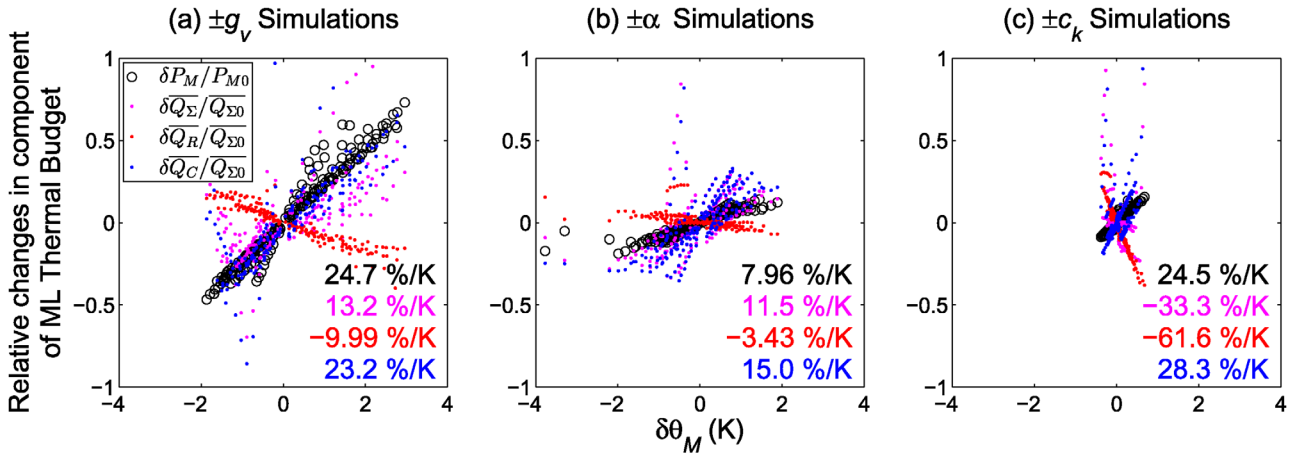

Figure 10. Fractional changes in the components of ML thermal balance, $\delta P_M/P_{M0}$ and $\delta\overline{Q_\Sigma}/\overline{Q_{\Sigma0}}$, as given by equation (43), plotted against changes in θ_M, for RC model simulations with no cloud-radiation interactions or diurnal cycle. The change in total ML cooling rate per unit mass, $\delta\overline{Q_\Sigma}/\overline{Q_{\Sigma0}}$, is made up of radiative $(\delta\overline{Q_R}/\overline{Q_{\Sigma0}})$ and convective $(\delta\overline{Q_C}/\overline{Q_{\Sigma0}})$ components. Subfigures are for perturbations of individual surface parameters (a) $\pm g_v$, (b) $\pm\alpha$, and (c) $\pm c_k$, as described in the text. Linear regression of fractional changes of each of the plotted variables provides the slopes given in colored text at the bottom right of each subfigure.

increase in convective cooling (the $\overline{Q_C}/\overline{Q_{\Sigma 0}}$ term) with increasing θ_M is consistent with more evaporation of rain in a deeper, drier ML. Only in the case of $\pm g_v$ simulations do changes in ML depth (the $\delta P_M/P_{M0}$ term) dominate changes in cooling rate of the ML, which helps to explain why $\pm g_v$ simulations are fit best by the theory. Ultimately, these significant deviations from constant ML cooling rate do not present an insurmountable problem for the validity of our theory, because the constant cooling rate assumption is largely embedded in the value of γ. Despite the appearance of γ in a number of places throughout the theory, it rarely dominates the full expression for the sensitivity of T_S or θ_M, since it is generally small ($\sim$0.2) compared to the factor of 1 to which it is added in the expression for λ_E. For the $\pm\alpha$ simulations, the nontrivial changes in θ above the ML (as discussed in section 4.3) help to explain why $\delta P_M/P_{M0}$ in Figure 10b has a lower slope as a function of $\delta\theta_M$ than in Figures 10a and 10c. A significant part of the change in θ_M for the $\pm\alpha$ simulations is unrelated to changes in P_M and occurs simply due to warming of the lower free troposphere.

[78] Another limitation is less visible in the simulation results we have shown but has somewhat constrained our exploration of parameter space. Generally speaking, the key assumption of a constant θ_T profile is violated in the RC model if there is an abrupt change between deep convection and no deep convection in one column or the other; with similar but more dramatic results than the abrupt changes that were shown when cloud-radiation interactions were enabled. In order to attempt to avoid such cases (which we view as somewhat artificial, related to discretization and the limited number of columns), we have filtered our results for active deep convection in both columns (as diagnosed by a significantly nonzero time-mean updraft mass flux at 700 hPa), and we have also attempted to choose parameters and reference states that ensure some deep convection in both columns. This requirement unfortunately limits the accessibility of surfaces with very low values of g_v, which would theoretically have high sensitivity to further drying (or other surface parameter changes).

[79] The assumption of a constant θ_T profile, including constant Γ, also prevents the theory from being applied in its present state to perturbations that cause warming or cooling, or affect the lapse rate, of the free troposphere. This means that changes in ML structure due to the long-term effects of CO_2 as a global greenhouse gas will not be captured by the theory we have presented. Sensitivity of boundary layer temperatures to free-tropospheric temperatures is an important problem not only from the standpoint of climate change but also from a standpoint of understanding how the coupled surface-ML system acts to amplify or dampen synoptic variability, as in heat waves. In its current form, the theory may be useful for understanding the fast component of CO_2-driven greenhouse warming, where land warms but sea surface temperatures remain nearly fixed [*Dong et al.*, 2009; *Wyant et al.*, 2012]. Since such warming is driven by a simple longwave radiative perturbation to the surface energy budget, we could calculate the theoretical response by simply plugging in the surface longwave radiative forcing of a step change in CO_2 to the general sensitivity equation (22). As we will discuss later, the theory may also be useful for understanding the nonradiative implications of changes in CO_2 on the surface energy balance (i.e., physiological forcing). It is possible to modify the theory to allow for forcings that impact the free-tropospheric temperature profile, by modifying equation (15) to include a term $\partial\theta_T/\partial A$. We have not included this term because it makes the subsequent derivation more algebraically cumbersome ($\mathrm{d}q_M/\mathrm{d}A$ is no longer related to $\mathrm{d}\theta_M/\mathrm{d}A$ by a simple multiplicative factor) than is considered worthwhile for this paper. The calculation of equilibrium boundary layer sensitivity to free-tropospheric temperature represents less an inherent limitation of theory than an opportunity for future valuable work.

[80] A final limitation of the theory is likely evident: by using as the basis for our theory an equilibrium model with diurnally averaged solar forcing, we do not take into account any nonlinearities associated with the diurnal cycle, which could alter the quantitative sensitivities of the time-mean thermal structure of the boundary layer to the time-mean of the surface fluxes. This might occur in a meaningful way for our theory, for example, if forcings and feedbacks covaried in time (over the course of the day) significantly enough that the covariance terms were large compared to the time-mean terms (our theory considers only the time-mean terms). As noted by B00, it appears that the equilibrium mixed layer model can explain a substantial amount of the variability in daily-average surface temperatures across two basins in the midwestern United States, so there is reason to hope that diurnal nonlinearities are not overwhelming. We have also shown that the sensitivity theory still appears to compare favorably with the time-mean solutions from RC model simulations obtained with diurnally varying radiation, though the theory as applied to $\pm\alpha$ and $\pm c_k$ simulations has reduced skill (Figure 9). The similarity of the climatic and diurnal cycle equilbria from *Brubaker and Entekhabi* [1995] lends additional support to the hypothesis that diurnal nonlinearities are not of critical importance for daily-average temperatures. While these are all encouraging signs, neither our simulations with diurnally varying radiation nor the work of *Brubaker and Entekhabi* [1995] adequately parameterizes many important aspects of the stable nocturnal boundary layer. The importance of diurnal nonlinearities for our theory, especially those associated with the stable nocturnal boundary layer, remains an important and open question for future research.

5.2. Precipitation, Convection, and Clouds

[81] Plotting changes in precipitation against changes in evaporation reveals a great deal of similarity among the set of simulations with no cloud-radiation interactions and no diurnal cycle (Figure 11). Simulations where g_v or c_k are varied roughly obey the simple scaling that $\delta P \approx \delta E$—precipitation changes approximately

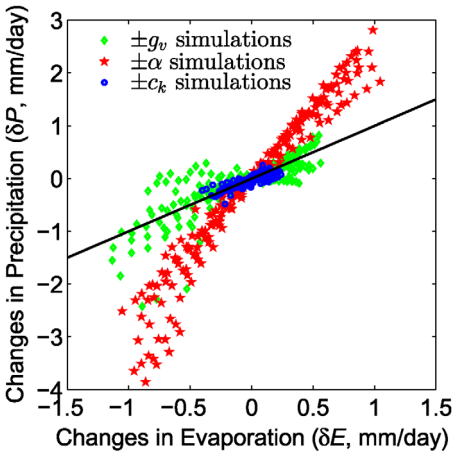

Figure 11. Scatterplot of changes in precipitation (δP, mm/day) against changes in evaporation (δE, mm/day) for RC model simulations with no cloud-radiation interactions or diurnal cycle. The black diagonal line indicates $\delta P = \delta E$, which is followed roughly for $\pm g_v$ and $\pm c_k$ simulations, but not $\pm\alpha$ simulations, where precipitation changes much more rapidly than evaporation due to changes in overturning circulation strength.

equal evaporation changes. This rough equality holds because changes in moisture convergence by the two-column overturning circulation are small for $\pm g_v$ and $\pm c_k$ simulations. Rough equality of changes in precipitation and evaporation fails to hold for $\pm\alpha$ simulations, where δP changes much more rapidly than δE. Changes in land surface albedo affect atmospheric column energy balance, and thus the moisture converged by overturning circulations, much more strongly than do changes in surface roughness or vegetation conductance. Figure 11 also helps to show the typical scales of sensitivity of precipitation to the three land surface parameters. Changes in precipitation are quite small for $\pm c_k$ simulations, intermediate for $\pm g_v$ simulations, and large for $\pm\alpha$ simulations, with the standard deviation of $\sigma_{\delta P} \sim 0.1$, 0.5, and 1.5 mm/d for the three surface parameters, respectively (averaged across all atmospheric boundary conditions).

[82] In simulations where albedo is varied, subcloud quasiequilibrium [*Raymond*, 1995] provides a useful theory with which to diagnose changes in cumulus mass fluxes and, to some extent, precipitation rates. Specifically, we expect that the updraft mass flux at cloud base M_u should equal the large-scale vertical mass flux at cloud base, $-\omega/g$, plus a term related to the surface fluxes divided by the column-average saturation static energy (SSE) deficit:

$$M_u = -\omega/g + \frac{H+E}{b\left(\overline{h^*} - \overline{h}\right)}. \tag{44}$$

[83] Here, b is an unknown factor relating the average SSE deficit in the free troposphere, $\overline{h^*} - \overline{h}$, to the average SSE deficit in downdrafts. With $b \sim 2$, the RHS and LHS of (44) agree, as diagnosed from model output. In simulations with varying albedo, we find empirically that we can diagnose changes in precipitation by the approximation:

$$\delta P \sim \delta(M_u q_M). \tag{45}$$

[84] In other words, for $\pm\alpha$ simulations, changes in precipitation, δP, appear to scale with changes in the product of cloud base mass flux (M_u)—itself dependent on the total turbulent surface enthalpy flux $H + E$ via 44—and boundary layer specific humidity (q_M).

[85] The RC model simulations with interactions between clouds and radiation allow us to estimate the shortwave feedback λ_{Q_S}, and to understand whether our null assumption regarding it has significantly affected our theory. We diagnose λ_{Q_S} by linear regression of δQ_S against $\delta\theta_M$ (correcting for any changes in Q_S that are due to changes in α). We find that shortwave feedbacks are a modest but significant positive feedback for $\pm g_v$ and $\pm c_k$ simulations but a strongly negative feedback for $\pm\alpha$ simulations. A linear model $\delta Q_S = \lambda_{Q_S}\delta\theta_M$ explains the vast majority (80–95%) of the variance in δQ_S, and gives $\lambda_{Q_S} \approx (+6.8, -36.5, +8.6)\mathrm{W/m^2/K}$, for $\pm(g_v, \alpha, c_k)$ simulations, respectively. These results suggest that warming due to reduced g_v or c_k leads to less cloudiness and that warming due to decreased α leads to more cloudiness. Clearly, the concept of forcing-independent feedbacks does not apply in the case of λ_{Q_S}. For both g_v and c_k, the inferred values for λ_{Q_S} are considerably smaller than the typical values of λ_E, so the theory still captures most of the variance in $\delta\theta_M$ and δT_S, even with the assumption $\lambda_{Q_S} = 0$. For α, the value of λ_{Q_S} is quite large, and would tend to make changes in θ_M smaller than our theory would predict with $\lambda_{Q_S} = 0$. We instead see the opposite bias: our theory underestimates the magnitude of $\delta\theta_M$ in Figure 8 because of the compensating effects of free-tropospheric temperature changes in $\pm\alpha$ simulations, a somewhat fortuitous cancellation. These results regarding shortwave effects of cloud changes warrant some skepticism, because there is no separate parameterization of shallow cumulus convection in the model; it is likely unrealistic that simulated changes in net shortwave radiation occur principally due to changes in deep clouds.

5.3. Applications

[86] The theory presented here potentially has broad quantitative applications to changes in climate driven by land cover changes. Whether land cover change is anthropogenic or natural, it will almost invariably result in concurrent changes in conductance to water vapor, albedo, and surface roughness. Here we will discuss one application, to the subject of changes in climate driven by stomatal closure under elevated CO_2, which has been termed "physiological forcing" of CO_2 by *Betts et al.* [2004] and others [e.g., *Boucher et al.*, 2009; *Cao et al.*, 2009, 2010; *Betts and Chiu*, 2010; *Andrews et al.*, 2011].

[87] Numerous experimental studies have found that stomata, the pores in the leaves of plants through which

Table 5. Survey of Studies Examining the Climate Impacts of Physiological Forcing of Elevated CO_2, as in Table 2 of *Cao et al.* [2010][a]

Study, Models Used	ΔT_r	ΔT_{rp}	ΔT_{rp-r}	$\%\frac{\Delta T_{rp-r}}{\Delta T_{rp}}$
Sellers et al. [1996], SiB2-CSU GCM	2.6	2.8	**0.2**	7
Cox et al. [1999], MOSES-HadCM2	3.06	3.45	**0.39**	11
Notaro et al. [2007],[b] LPJ-PCCM3	2.3	2.7	**0.4**	15
Boucher et al. [2009], MOSES-HadCM3	3.51	4.03	**0.52**	13
Cao et al. [2009], CLM3.0-CAM3.1	2.35	2.47	**0.12**	5
Cao et al. [2010], CLM3.5-CAM3.5	2.86	3.33	**0.47**	14
Andrews et al. [2011],[c] HadCM3LC	0.49	1.31	**0.82**	63

[a]ΔT_r: average warming (K) over land due to radiative effects of elevated CO_2; ΔT_{rp}: average warming (K) over land due to radiative plus physiological effects of elevated CO_2. Difference ΔT_{rp-r} (K) is attributed to physiological forcing of CO_2, with values set in bold for emphasis.

[b]*Notaro et al.* [2007] also includes changes in leaf area index and vegetation cover.

[c]*Andrews et al.* [2011] is for fast response (limit of no change in SST) only, for $4\times CO_2$.

water vapor and CO_2 are exchanged with the atmosphere, tend to close, or reduce in number, as the atmospheric CO_2 concentration increases [e.g., *Field et al.*, 1995; *Medlyn et al.*, 2001; *Lammertsma et al.*, 2011]. Other things being equal, this implies a decrease in g_v as CO_2 rises. Several studies have used GCMs to address the question of how much of the warming signal due to elevated CO_2 in model projections can be attributed to the physiological effects of changes in CO_2, typically by contrasting two simulations, both with elevated CO_2. In one simulation, the radiation module of the code sees the elevated CO_2, but the plant physiology module does not; this gives the temperature change due to radiative forcing by CO_2 (ΔT_r in Table 5). In the other simulation, both the radiation and plant physiology modules see the elevated CO_2; this gives the temperature change due to both radiative and physiological forcing of CO_2 (ΔT_{rp} in Table 5). The difference between these two simulations is considered the climate response to the physiological forcing of elevated CO_2, and is denoted ΔT_{rp-r} in the bolded column of Table 5). *Cao et al.* [2010] cite a subset of the studies summarized in Table 5 as representing "an emerging consensus" on the climate impacts of physiological forcing, with the physiological forcing due to a doubling of CO_2 leading to a rise in average surface air temperatures over land of ~0.4 K; the multimodel mean from the bolded column of Table 5 is 0.35 K (halving the result from *Andrews et al.* [2011] from a $4xCO_2$ perturbation). Our estimate at the end of section 2.5 suggested that a 10% change in $\beta = g_v/(g_a+g_v)$ might be expected to lead to roughly a 0.29 K warming over a moist surface. Using reference-state values of $g_v = 0.008$ m/s and $g_a = 0.025$ m/s, the 20% decrease in g_v under elevated CO_2 reported by *Medlyn et al.* [2001] would translate to a 16% reduction in β, and thus to roughly a 0.5 K warming, similar to the set of GCM results. This, of course, is an extremely crude estimate, as it ignores many of the details of geographic structure that are found in GCM simulations, and no calculation of average g_v over land has been made to justify the use of a moist surface rather than a dry one. The recent studies of *Doutriaux-Boucher et al.* [2009] and *Vila-Guerau de Arellano et al.* [2012] also suggest that changes in clouds can be an important aspect of the global response to physiological forcing by CO_2; we have not considered such changes here.

[88] We also may be able to use our theory to understand why the results of *Betts and Chiu* [2010]—approximately a 4 K increase in a doubled-CO_2 scenario—are so much larger than the "emerging consensus" suggested by Table 5. First, the reduction in g_v in their study is quite large—roughly 60−70%—compared to what is typically found by GCMs. Second, in spite of a low reference-state $g_v \sim 0.003\mathrm{m/s}$, their model still has a value of $E_0 \approx 113\mathrm{W/m^2}$. This results in an extremely large forcing of ~115 W/m^2 (note that for very large changes in g_v, the forcing can exceed the reference-state latent heat flux, since the magnitude of the logarithmic term in (29) can exceed 1). Because the reference value of g_{v0} in *Betts and Chiu* [2010] is so small, their evaporative feedback is relatively weak; we estimate $\lambda_E \sim 19\mathrm{W/m^2/K}$. Together with a sensible heat flux feedback of ~6 W/m^2/K (as above), this gives a very large expected warming, of ~4.6 K. This is larger than the additional warming of 4 K that they simulate, likely because of differences in the values of γ and ξ, and the potential for numerical errors in estimation from graphs. Our theory thus suggests that a combination of a large forcing, together with a relatively weak evaporative feedback, is likely the essential mechanism that gives rise to the "unrealistically large" climate response to physiological forcing in the study of *Betts and Chiu* [2010].

6. Conclusions

[89] We have briefly presented a framework for calculating the boundary layer climate sensitivity and then developed in detail a analytic theory of boundary layer climate sensitivity, based on the diurnally averaged model of B00. The theory is developed analogously to climate sensitivity, but based on surface energy balance, rather than top-of-atmosphere energy balance. The theory identifies forcings associated with changes in land surface properties, including conductance to water vapor, albedo, and aerodynamic roughness, and identifies feedbacks associated with each of the four components of surface energy balance (latent and sensible turbulent heat fluxes, longwave and shortwave radiative fluxes). As in the work of *Brubaker and Entekhabi* [1996] and *Kim and Entekhabi* [1998], we find that a strongly negative evaporative feedback (λ_E), related to the dependence of saturation specific humidity on temperature, usually plays the dominant role in limiting the response of surface temperatures to a perturbation in surface properties. We find extremely good agreement between the theory and the more complex set of equations from B00 on which it is based and find that allowing for forcings that are nonlinear functions of surface properties is

key to obtaining good agreement for large perturbations in surface properties. The importance of nonlinear forcings represents an interesting further analogy to climate sensitivity. We have also performed simulations with a two-column RC model with many more degrees of freedom, which supports the general utility of the theory even when many of the assumptions upon which it is based are no longer strictly enforced.

[90] Although the theory has a number of limitations, we believe that it may be broadly useful for unifying our understanding of how changes in land use or ecosystem function may affect changes in climate. As an example case, we explore the application of the theory to the problem of climate change driven by suppression of surface conductance to water vapor under elevated CO_2 (physiological forcing). We find that our theory provides a reasonable estimate of the warming simulated by past studies that have used global models, and may help to explain why the warming in the simpler study of *Betts and Chiu* [2010] is so large. Directions for future work include application to problems such as urbanization, agricultural expansion, and afforestation, as well as extension of the theory to examine forcing by free-tropospheric temperature change. Even if the quantitative expressions for feedbacks and forcings presented here prove to be quite different from those calculated from GCMs, we hope that the framework of boundary layer climate sensitivity will help to standardize how climate changes induced by land cover changes are assessed in modeling studies.

Appendix A: Details of Sensitivity Theory

A1. Derivation of ξ

[91] Here, we derive ξ, the parameter relating changes in q_M to changes in θ_M in equation (20). Expanding (19) gives

$$\frac{dq_M}{dA} = \frac{\epsilon}{p_b}\frac{\partial e^*}{\partial T}\Big|_{T_b}\frac{dT_b}{dA} - \frac{\epsilon e^*(T_b)}{p_b^2}\frac{dp_b}{dA}. \tag{A1}$$

[92] Using (15) and the definition of $p_b = p_s - P_M$, we can replace $\mathrm{d}p_b/\mathrm{d}A$ with $-\Gamma(\mathrm{d}\theta_M/\mathrm{d}A)$. Using the definition of T_b from (18), we have

$$\begin{aligned}\frac{\mathrm{d}T_b}{\mathrm{d}A} &= \left(\frac{p_b}{p_s}\right)^{\frac{R}{c_p}}\left(\frac{\mathrm{d}\theta_M}{\mathrm{d}A} + \frac{R\theta_M}{c_p p_b}\frac{\mathrm{d}p_b}{\mathrm{d}A}\right)\\ &= \left(\frac{p_b}{p_s}\right)^{\frac{R}{c_p}}\left(1 - \frac{R\theta_M}{c_p p_b \Gamma}\right)\frac{\mathrm{d}\theta_M}{\mathrm{d}A}.\end{aligned} \tag{A2}$$

[93] Putting this back into (A1) gives

$$\frac{\mathrm{d}q_M}{\mathrm{d}A} = \left[\frac{\partial q^*}{\partial T}\Big|_{T_b}\left(\frac{p_b}{p_s}\right)^{\frac{R}{c_p}}\left(1 - \frac{R\theta_M}{c_p p_b \Gamma}\right) + \frac{q_M}{p_b \Gamma}\right]\frac{\mathrm{d}\theta_M}{\mathrm{d}A}, \tag{A3}$$

where we have again used $q^* = \epsilon e^*/p$ and $q_M = q^*(T_b, p_b)$ to simplify the expression. The term in square brackets in (A3) is defined as ξ.

A2. Expansion of Surface Energy Balance

[94] The total derivatives in (4) can be expanded by the chain rule

$$\frac{\mathrm{d}Q_S}{\mathrm{d}A} = \frac{\partial Q_S}{\partial A} + \frac{\partial Q_S}{\partial T_S}\frac{\mathrm{d}T_S}{\mathrm{d}A} + \frac{\partial Q_S}{\partial \theta_M}\frac{\mathrm{d}\theta_M}{\mathrm{d}A} + \frac{\partial Q_S}{\partial q_M}\frac{\mathrm{d}q_M}{\mathrm{d}A} \tag{A4}$$

$$\frac{\mathrm{d}Q_L}{\mathrm{d}A} = \frac{\partial Q_L}{\partial A} + \frac{\partial Q_L}{\partial T_S}\frac{\mathrm{d}T_S}{\mathrm{d}A} + \frac{\partial Q_L}{\partial \theta_M}\frac{\mathrm{d}\theta_M}{\mathrm{d}A} + \frac{\partial Q_L}{\partial q_M}\frac{\mathrm{d}q_M}{\mathrm{d}A} \tag{A5}$$

$$\frac{\mathrm{d}H}{\mathrm{d}A} = \frac{\partial H}{\partial A} + \frac{\partial H}{\partial T_S}\frac{\mathrm{d}T_S}{\mathrm{d}A} + \frac{\partial H}{\partial \theta_M}\frac{\mathrm{d}\theta_M}{\mathrm{d}A} + \frac{\partial H}{\partial q_M}\frac{\mathrm{d}q_M}{\mathrm{d}A} \tag{A6}$$

$$\frac{\mathrm{d}E}{\mathrm{d}A} = \frac{\partial E}{\partial A} + \frac{\partial E}{\partial T_S}\frac{\mathrm{d}T_S}{\mathrm{d}A} + \frac{\partial E}{\partial \theta_M}\frac{\mathrm{d}\theta_M}{\mathrm{d}A} + \frac{\partial E}{\partial q_M}\frac{\mathrm{d}q_M}{\mathrm{d}A}. \tag{A7}$$

[95] For a typical choice of A, many of these terms vanish, but all are retained here for generality. We can eliminate $\mathrm{d}T_S/\mathrm{d}A$ and $\mathrm{d}q_M/\mathrm{d}A$ from these expressions in favor of $\mathrm{d}\theta_M/\mathrm{d}A$, using (16) and (20). After rearranging to move the differential $\mathrm{d}A$ to the right-hand side, this gives

$$\begin{aligned}\mathrm{d}Q_S &= \left(\frac{\partial Q_S}{\partial A} - \frac{1}{\rho c_p g_a}\frac{\partial Q_S}{\partial T_S}\frac{\partial H}{\partial A}\right)\mathrm{d}A\\ &\quad + \left((1+\gamma)\frac{\partial Q_S}{\partial T_S} + \frac{\partial Q_S}{\partial \theta_M} + \xi\frac{\partial Q_S}{\partial q_M}\right)\mathrm{d}\theta_M\\ &\equiv \mathrm{d}F_{Q_S}^A + \lambda_{Q_S}\mathrm{d}\theta_M\end{aligned} \tag{A8}$$

$$\begin{aligned}\mathrm{d}Q_L &= \left(\frac{\partial Q_L}{\partial A} - \frac{1}{\rho c_p g_a}\frac{\partial Q_L}{\partial T_S}\frac{\partial H}{\partial A}\right)\mathrm{d}A\\ &\quad + \left((1+\gamma)\frac{\partial Q_L}{\partial T_S} + \frac{\partial Q_L}{\partial \theta_M} + \xi\frac{\partial Q_L}{\partial q_M}\right)\mathrm{d}\theta_M\\ &\equiv \mathrm{d}F_{Q_L}^A + \lambda_{Q_L}\mathrm{d}\theta_M\end{aligned} \tag{A9}$$

$$\begin{aligned}\mathrm{d}H &= \left(\frac{\partial H}{\partial A} - \frac{1}{\rho c_p g_a}\frac{\partial H}{\partial T_S}\frac{\partial H}{\partial A}\right)\mathrm{d}A\\ &\quad + \left((1+\gamma)\frac{\partial H}{\partial T_S} + \frac{\partial H}{\partial \theta_M} + \xi\frac{\partial H}{\partial q_M}\right)\mathrm{d}\theta_M\\ &\equiv \mathrm{d}F_H^A + \lambda_H\mathrm{d}\theta_M\end{aligned} \tag{A10}$$

$$\begin{aligned}\mathrm{d}E &= \left(\frac{\partial E}{\partial A} - \frac{1}{\rho c_p g_a}\frac{\partial E}{\partial T_S}\frac{\partial H}{\partial A}\right)\mathrm{d}A\\ &\quad + \left((1+\gamma)\frac{\partial E}{\partial T_S} + \frac{\partial E}{\partial \theta_M} + \xi\frac{\partial E}{\partial q_M}\right)\mathrm{d}\theta_M\\ &\equiv dF_E^A + \lambda_E d\theta_M,\end{aligned} \tag{A11}$$

where the terms including a factor of dA (A8)–(A11) have been defined as differential forcings ($\mathrm{d}F_{Q_S}^A$, $\mathrm{d}F_{Q_L}^A$, $\mathrm{d}F_H^A$, and $\mathrm{d}F_E^A$) and the terms multiplying the differential change in potential temperature, $\mathrm{d}\theta_M$, have been defined as feedbacks ($\lambda_{Q_S}, \lambda_{Q_L}, \lambda_H$, and λ_E). Note that we have kept the symmetry of the equations for clarity, but we can make one general simplification immediately from the definition of H: $\mathrm{d}F_H^A = 0$, since

$\partial H/\partial T_S = \rho c_p g_a$. However, the impacts of $\partial H/\partial A$ are distributed over the other terms $\mathrm{d}F^A_{Q_S}$, $\mathrm{d}F^A_{Q_L}$, and $\mathrm{d}F^A_E$.

[96] Now, applying surface energy balance (3), we can obtain

$$\mathrm{d}Q_S - \mathrm{d}Q_L - \mathrm{d}H - \mathrm{d}E = 0 \tag{A12}$$

$$\mathrm{d}F^A_{Q_S} - \mathrm{d}F^A_{Q_L} - \mathrm{d}F^A_E + \left(\lambda_{Q_S} - \lambda_{Q_L} - \lambda_H - \lambda_E\right)\mathrm{d}\theta_M = 0 \tag{A13}$$

$$\frac{\mathrm{d}F^A_{Q_S} - \mathrm{d}F^A_{Q_L} - \mathrm{d}F^A_E}{\lambda_{Q_L} + \lambda_H + \lambda_E - \lambda_{Q_S}} = \mathrm{d}\theta_M, \tag{A14}$$

where the last step has assumed the feedbacks are nearly constant so that we can rearrange them before integration. Integration of $\mathrm{d}\theta_M$ simply yields $\theta_M - \theta_{M0} \equiv \delta\theta$. Full integration of the differential forcings gives the results quoted in the main text, equation (23). We could also assume that the forcings were linear in $A - A_0 \equiv \delta A$, so that

$$\begin{aligned} F^A_{Q_S,lin} &\equiv \left(\frac{\partial Q_S}{\partial A} - \frac{1}{\rho c_p g_a}\frac{\partial Q_S}{\partial T_S}\frac{\partial H}{\partial A}\right)\delta A \\ F^A_{Q_L,lin} &\equiv \left(\frac{\partial Q_L}{\partial A} - \frac{1}{\rho c_p g_a}\frac{\partial Q_L}{\partial T_S}\frac{\partial H}{\partial A}\right)\delta A \\ F^A_{E,lin} &\equiv \left(\frac{\partial E}{\partial A} - \frac{1}{\rho c_p g_a}\frac{\partial E}{\partial T_S}\frac{\partial H}{\partial A}\right)\delta A \end{aligned} \tag{A15}$$

[97] In parallel with the nonlinear-forcing derivations of sections 2.5–2.7, expressions for total linear forcings with $A \rightarrow (g_v, \alpha, g_a)$ are given by

$$\begin{aligned} F^{g_v}_{lin} &= \frac{g_a}{g_a + g_{v0}} E_0 \frac{\delta g_v}{g_{v0}} \\ F^{\alpha}_{lin} &= -\frac{Q_{S0}}{1-\alpha_0}\delta\alpha \\ F^{g_a}_{lin} &= \frac{g_v}{g_{a0}+g_v}\left(E_0 - \frac{H_0}{B_e}\right)\frac{\delta g_a}{g_{a0}} - \frac{4\sigma_B T^3_{S0} H_0}{\rho c_p g_{a0}}\frac{\delta g_a}{g_{a0}}. \end{aligned} \tag{A16}$$

[98] For brevity here, we have summed the forcings from different surface fluxes. As discussed in section 3, the usage of linear forcings is generally inferior to the use of the fully nonlinear forcings described in detail in sections 2.5–2.7 and Table 2. We include the expressions for linear forcings here to clarify the methodology underlying the calculation of the results shown in Figures 2 and 3.

[99] **Acknowledgments.** I would like to thank Kerry Emanuel for many conversations about this work, as well as for supplying me with the radiative-convective model on which much of the evaluation of the theory is based. Peter Molnar, Mike Byrne, Jack Scheff, and two anonymous reviewers, all provided numerous useful comments and critiques on various drafts of this work. Alan Betts generously and rapidly shared the quantitative results from *Betts* [2000], which allowed for confirmation that my solutions reproduce his. This work was funded by NSF grant 1136480, The Effect of Near-Equatorial Islands on Climate. Preliminary versions of this work were aided by conversations with Ron Prinn and Adam Schlosser, and funded by grants from the DOE (DE-FG02–94ER61937) and EPRI (EP-P8155/C4107), as well as by a supporting research award for the Joint Program on the Science and Policy of Global Change.

References

Abbot, D., and K. Emanuel (2007), A tropical and subtropical land–sea–atmosphere drought oscillation mechanism, *J. Atmos. Sci.*, *64*, 4458–4468, doi:10.1175/2007JAS2186.1.

Allen, R., L. Pereira, D. Raes, and M. Smith (1998), *Crop evapotranspiration: Guidelines for computing crop water requirements, Irrig. Drain. Pap. 56*, 300 pp., United Nations FAO, Rome.

Andrews, T., M. Doutriaux-Boucher, O. Boucher, and P. Forster (2011), A regional and global analysis of carbon dioxide physiological forcing and its impact on climate, *Clim. Dyn.*, *36*, 783–792, doi:10.1007/s00382-010-0742-1.

Betts, A. (2000), Idealized model for equilibrium boundary layer over land, *J. Hydrometeorol.*, *1*, 507–523.

Betts, A., and J. Chiu (2010), Idealized model for changes in equilibrium temperature, mixed layer depth, and boundary layer cloud over land in a doubled CO_2 climate, *J. Geophys. Res.*, *115*, D19108, doi:10.1029/2009JD012888.

Betts, A., and W. Ridgway (1988), Coupling of the radiative, convective, and surface fluxes over the equatorial pacific, *J. Atmos. Sci.*, *45*, 522–536.

Betts, A., and W. Ridgway (1989), Climatic equilibrium of the atmospheric convective boundary layer over a tropical ocean, *J. Atmos. Sci.*, *46*, 2621–2641.

Betts, R., P. Cox, M. Collins, P. Harris, C. Huntingford, and C. Jones (2004), The role of ecosystem-atmosphere interactions in simulated Amazonian precipitation decrease and forest dieback under global climate warming, *Theor. Appl. Climatol.*, *78*, 157–175, doi:10.1007/s00704-004-0050-y.

Boucher, O., A. Jones, and R. Betts (2009), Climate response to the physiological impact of carbon dioxide on plants in the Met Office Unified Model HadCM3, *Clim. Dyn.*, *32*, 237–249, doi:10.1007/s00382-008-0459-6.

Bony, S., and K. Emanuel (2001), A parameterization of the cloudiness associated with cumulus convection; Evaluation using TOGA COARE data, *J. Atmos. Sci.*, *58*, 3158–3183.

Brubaker, K., and D. Entekhabi (1995), An analytic approach to modeling land-atmosphere interaction: 1. Construct and equilibrium behavior, *Water Resour. Res.*, *31*, 619–632.

Brubaker, K., and D. Entekhabi (1996), Analysis of feedback mechanisms in land-atmosphere interaction, *Water Resour. Res.*, *32*, 1343–1357.

Cao, L., G. Bala, K. Caldeira, R. Nemani, and G. Ban-Weiss (2009), Climate response to physiological forcing of carbon dioxide simulated by the coupled community atmosphere model (CAM3.1) and community land model (CLM3.0), *Geophys. Res. Lett.*, *36*, L10402, doi:10.1029/2009GL037724.

Cao, L., G. Bala, K. Caldeira, R. Nemani, and G. Ban-Weiss (2010), Importance of carbon dioxide physiological forcing to future climate change, *Proc. Natl. Acad. Sci. U. S. A.*, *107*, 9513–9518, doi:10.1073/pnas.0913000107.

Charney, J. (1975), Dynamics of deserts and drought in the Sahel, *Q. J. R. Meteorol. Soc.*, *101*, 193–202.

Cox, P., R. Betts, C. Bunton, R. Essery, P. Rowntree, and J. Smith (1999), The impact of new land surface physics on the GCM simulation of climate and climate sensitivity, *Clim. Dyn.*, *15*, 183–203.

Dong, B., J. Gregory, and R. Sutton (2009), Understanding land-sea warming contrast in response to increasing greenhouse gases. Part I: Transient adjustment, *J. Clim.*, *22*, 3079–3097, doi:10.1175/2009JCLI2652.1.

Doutriaux-Boucher, M., M. Webb, J. Gregory, and O. Boucher (2009), Carbon dioxide induced stomatal closure increases radiative forcing via a rapid reduction in low cloud, *Geophys. Res. Lett.*, *36*, L02703, doi:10.1029/2008GL036273.

Emanuel, K., and M. Zivkovic-Rothman (1999), Development and evaluation of a convection scheme for use in climate models, *J. Atmos. Sci.*, *56*, 1766–1782.

Entekhabi, D., and K. Brubaker (1995), An analytic approach to modeling land-atmosphere interaction: 2. Stochastic formulation, *Water Resour. Res.*, *31*, 633–643.

Field, C., R. Jackson, and H. Mooney (1995), Stomatal responses to increased CO2: Implications from the plant to the global scale, *Plant Cell Environ.*, *18*, 1214–1225.

Hartmann, D. (1994), *Global Physical Climatology, Int. Geophys. Ser.*, vol. *56*, 409 pp., Academic Press, San Diego.

Held, I. (2005), The gap between simulation and understanding in climate modeling, *Bull. Am. Meteorol. Soc.*, *80*, 1609–1614, doi:10.1175/BAMS-86-11-1609.

Jacobs, C., and H. De Bruin (1992), The sensitivity of regional transpiration to land-surface characteristics: Significance of feedback, *J. Clim.*, *5*, 683–698.

Jones, H. (1992), *Plants and Microclimate*, 2nd ed., 428 pp., Cambridge Univ. Press, Cambridge, U.K.

Kim, C., and D. Entekhabi (1998), Feedbacks in the land-surface and mixed-layer energy budgets, *Boundary Layer Meteorol.*, *88*, 1–21.

Lammertsma, E., H. de Boer, S. Dekker, D. Dilcher, A. Lotter, and F. Wagner-Cremer (2011), Global CO2 rise leads to reduced maximum stomatal conductance in florida vegetation, *Proc. Natl. Acad. Sci. U. S. A.*, *108*, 4035–4040, doi:10.1073/pnas.1100371108.

McNaughton, K., and T. Spriggs (1986), A mixed-layer model for regional evaporation, *Boundary Layer Meteorol.*, *34*, 243–262.

Medlyn, B., et al. (2001), Stomatal conductance of forest species after long-term exposure to elevated CO2 concentration: A synthesis, *New Phytolog.*, *149*, 247–264.

Monteith, J. (1965), Evaporation and environment, in *The State and Movement of Water in Living Organisms*, pp. 205–234, Cambridge Univ. Press, Cambridge, U.K.

Nilsson, J., and K. Emanuel (1999), Equilibrium atmospheres of a two-column radiative-convective model, *Q. J. R. Meteorol. Soc.*, *125*, 2239–2264.

Notaro, M., S. Vavrus, and Z. Liu, (2007), Global vegetation and climate change due to future increases in CO2 as projected by a fully coupled model with dynamic vegetation, *J. Clim.*, *20*, 70–90, doi:10.1175/JCLI3989.1.

Ramaswamy, V., O. Boucher, J. Haigh, D. Haughlustaine, J. Haywood, G. Myhre, T. Nakajima, G. Shi, S. Solomon, (2001), Radiative forcing of climate change, in *Climate Change 2001: The Scientific Basis. Contribution of Working Group I to the Third Assessment Report of the Intergovernmental Panel on Climate Change*, edited by J. T. Houghton et al., 881 pp., Cambridge Univ. Press, Cambridge, U. K.

Raymond, D. (1995), Regulation of moist convection over the west pacific warm pool, *J. Atmos. Sci.*, *52*, 3945–3959.

Sellers, P., et al. (1996), Comparison of radiative and physiological effects of doubled atmospheric CO2 on climate, *Science*, *271*, 1402–1406.

Shukla, J., and Y. Mintz (1982), Influence of land-surface evapotranspiration on the Earth's climate, *Science*, *215*, 1498–1501.

Sobel, A., J. Nilsson, and L. Polvani (2001), The weak temperature gradient approximation and balanced tropical moisture waves, *J. Atmos. Sci.*, *58*, 3650–3665.

Takahashi, K. (2009), Radiative constraints on the hydrological cycle in an idealized radiative-convective equilibrium model, *J. Atmos. Sci.*, *66*, 77–91, doi:10.1175/2008JAS2797.1.

Tennekes, H. (1973), A model for the dynamics of the inversion above a convective boundary layer, *J. Atmos. Sci.*, *30*, 558–567.

van Heerwaarden, C., J. Vila-Guerau de Arellano, A. Moene, and A. Holtslag (2009), Interactions between dry-air entrainment, surface evaporation and convective boundary-layer development, *Q. J. R. Meteorol. Soc.*, *135*, 1277–1291, doi:10.1002/qj.431.

van Heerwaarden, C., J. Vila-Guerau de Arellano, A. Gounou, F. Guichard, and F. Couvreux (2010), Understanding the daily cycle of evapotranspiration: A method to quantify the influence of forcings and feedbacks, *J. Hydrometeorol.*, *11*, 1405–1422, doi:10.1175/2010JHM1272.1.

Vila-Guerau de Arellano, J., C. van Heerwaarden, and J. Lelieveld (2012), Modelled suppression of boundary-layer clouds by plants in a CO2-rich atmosphere, *Nat. Geosci.*, *5*, 701–701, doi:10.1038/NGEO1554.

Wyant, C., C. Bretherton, P. Blossey, and M. Khairoutdinov (2012), Fast cloud adjustment to increasing CO2 in a superparameterized climate model, *J. Adv. Model. Earth Syst.*, *4*, M05001, doi:10.1029/2011MS000092.